



Universiteit  
Leiden  
The Netherlands

## How additives affect Cu electrodeposition : an electrochemical STM Study

Yanson, Y.I.

### Citation

Yanson, Y. I. (2012, December 4). *How additives affect Cu electrodeposition : an electrochemical STM Study. Casimir PhD Series*. Retrieved from <https://hdl.handle.net/1887/20221>

Version: Not Applicable (or Unknown)

License: [Leiden University Non-exclusive license](#)

Downloaded from: <https://hdl.handle.net/1887/20221>

**Note:** To cite this publication please use the final published version (if applicable).

Cover Page



Universiteit Leiden



The handle <http://hdl.handle.net/1887/20221> holds various files of this Leiden University dissertation.

**Author:** Yanson, Yuriy Igorevich

**Title:** How additives affect Cu electrodeposition : an electrochemical STM study

**Issue Date:** 2012-12-04

## Chapter 3

# Cu underpotential deposition on Au(111) and the effect of thiol-based additives

This chapter describes experiments and results on the first stage of Cu electrodeposition onto Au(111) surface, i.e. the Cu underpotential deposition (UPD). The electrolytes that are used in the experiments are similar to those utilized in commercial plating baths. The main focus of the chapter is on the effect of the additives, such as  $\text{Cl}^-$  and bis(3-sulfopropyl)disulfide (SPS), on the UPD process. Based on the experimental results, we propose a model that explains all the different observed stages of the UPD layer formation. Further, we show that this specific model of Cu UPD on Au(111) with SPS can be expanded to a more general case. We expect the model to be valid for the majority of systems, where the bond between the substrate and the thiol is adatom mediated. We also present different experimental observations, such as the lifting of the herringbone reconstruction on the Au(111) surface by Cu UPD and Cu UPD on a hexanethiol-modified Au(111) surface, which support the proposed general model. Finally, we present experimental observations of SPS adsorption on a preformed Cu UPD layer. These observations show that our model, while being generally correct, requires further refinements.

## 3.1 Introduction

In the past two decades, modification of metallic surfaces by organic molecules that contain an SH<sup>-</sup> function group, i.e. thiols, has drawn a lot of attention. These systems are interesting both from the fundamental and the application points of view. The fundamental interest lies in the interaction forces between the thiols and the metallic substrate, between thiol molecules themselves, and between the thiols and the electrolyte. It has been shown that a combination of these attractive and repulsive forces leads to the formation of a multitude of ordered interface structures, known as self-assembled monolayers (SAM). On the practical side, thiol molecules have, e.g., found application as surfactants in electroplating baths allowing a modification of the growth process and thereby of the properties of the deposit. For more information on both the fundamental aspects of SAM's and their practical use see recent reviews in [5, 68, 69].

A recent discovery, worth mentioning in the scope of the current chapter, is the adatom-mediated binding of thiol molecules to metal surfaces, in particular, to the Au(111) surface [6, 7, 70]. The rearrangement of the interface metal atoms upon thiol adsorption, which is sometimes referred to as thiol-SAM-induced surface reconstruction [71], is believed to lead to the formation of single vacancies in the metal surface. The rearrangement of these single vacancies by diffusion leads to the formation of the larger vacancy islands, which are observed experimentally [72–74]. However, there is still no clear consensus regarding this topic.

Different electrochemical, spectroscopic, and direct surface imaging techniques were employed to study metal deposition on metallic surfaces that have been modified by thiols. The *n*-alkanethiol SAM modified Au(111) surface has received the most attention as a model system for both underpotential and overpotential metal deposition [71, 75–84]. Also, COOH<sup>-</sup> [79, 85, 86], OH<sup>-</sup> [79, 87, 88] and SH<sup>-</sup> [87] terminated thiols have been studied. Furthermore, several studies have been conducted on metal deposition at surfaces modified by aromatic thiols [89–91]. Comparing different publications, one surprisingly finds that the results of different studies on similar systems vary and that they are sometimes even controversial. In particular, there is a debate concerning the processes, happening during copper underpotential deposition on thiol-modified Au(111) surfaces<sup>1</sup>

It is surprising that only a few studies have considered the structure of sulfonate-functionalized (SO<sub>3</sub>H<sup>-</sup>) thiol SAMs, such as bis(3-sulfopropyl)disulfide (SPS) or its monomer 3-mercapto-1-propanesulfonic acid (MPS) [93–98], as well as their effect on metal deposition [1, 99], despite their important practical application as surfactants for metal electrodeposition, e.g. during the metallization of semiconductor wafers.

In the present chapter we focus on the Cu underpotential deposition (UPD) on Au(111)

<sup>1</sup>For details see [23, 92] and references therein.

in the presence of SPS. We find that the UPD layer growth proceeds in two distinct steps. We show that this two step mechanism of the Cu UPD can be explained well by a simple model, if both the gold adatom-mediated thiol bond to the Au(111) surface and the morphology and growth of the Cu UPD layer are considered. Further, by means of several experiments as well as by pointing out examples from the literature, we show that our model can be applied to a variety of different systems exhibiting the UPD phenomenon, where the substrate is modified by a thiol.

## 3.2 Experimental details

All EC-STM measurements in this chapter were carried out with a Molecular Imaging PicoScan STM equipped with a PicoStat bi-potentiostat. A home-built quartz electrochemical flow cell was used, see Section 2.2.3.1. Either a copper wire or a palladium wire charged with hydrogen was used as a reference electrode and a gold wire served as a counter electrode. The *in situ* CV's were generally checked by additional measurements in a separate electrochemical cell using a dedicated potentiostat (Ivium Compact-Stat [100]) and a mercury/mercurous sulfate electrode (MSE) as a reference electrode. All potentials in this chapter refer to Cu/Cu<sup>2+</sup>, unless stated differently.

STM tips were prepared by electrochemical etching of a tungsten wire in a 2M NaOH aqueous solution by applying a DC voltage. After etching, the tips were coated with polyethylene to minimize faradaic currents. For more details on tip etching procedure as well as the sample preparation procedure see Appendix A.

## 3.3 Cu UPD from additive-free solutions

### 3.3.1 Sulfate containing electrolyte

Underpotential deposition of Cu on Au(111) from a sulfate containing solution is known to proceed in two steps. First, at a potential of about +250 mV a structure with 2/3 of a monolayer of Cu and 1/3 of a monolayer of coadsorbed sulfate is formed<sup>1</sup>. This UPD layer exhibits a ( $\sqrt{3} \times \sqrt{3}$ )R30° honeycomb structure, where the sulfate anions occupy the centers of the honeycomb, see Fig. 3.1a. At a more negative potential of about +25 mV the UPD layer transforms into a Cu-(1 × 1) pattern. There are only a few papers that estimate the surface coverage of the sulfate adlayer on top of the Cu-(1 × 1) structure: the reported values lie around 0.33 monolayer. Although the structure of this sulfate adlayer is unclear, it is suggested, on the basis of STM measurements, that the

<sup>1</sup>One monolayer corresponds to the surface concentration of gold atoms in an ideal, unreconstructed (111) surface ( $1.39 \times 10^{15}$  atoms/cm<sup>2</sup>).

sulfate forms a disordered mobile adlayer on the Cu-(1 × 1) structure. Figure 3.1 shows a model of the two different Cu UPD layer structures.

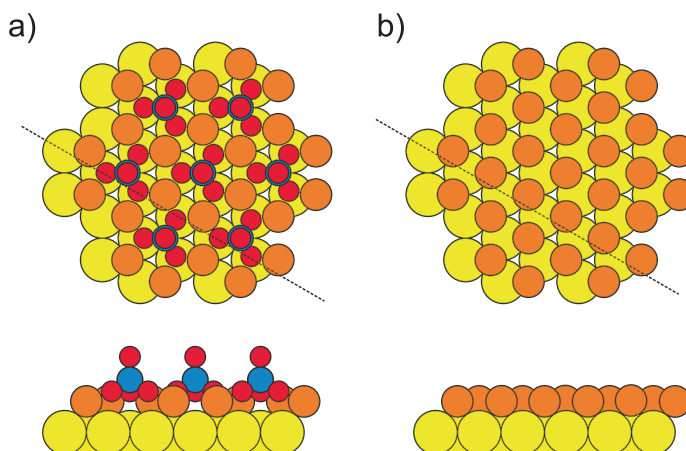


**Figure 3.1:** Atomic ball models of the Cu UPD layer structures on Au(111): (a) the  $(\sqrt{3} \times \sqrt{3})R30^\circ$  structure at +250 mV and (b) the  $(1 \times 1)$  structure +25 mV. The yellow, orange, blue, and red atoms correspond to gold, copper, sulfur, and oxygen, respectively. The image is reproduced with permission from [101].

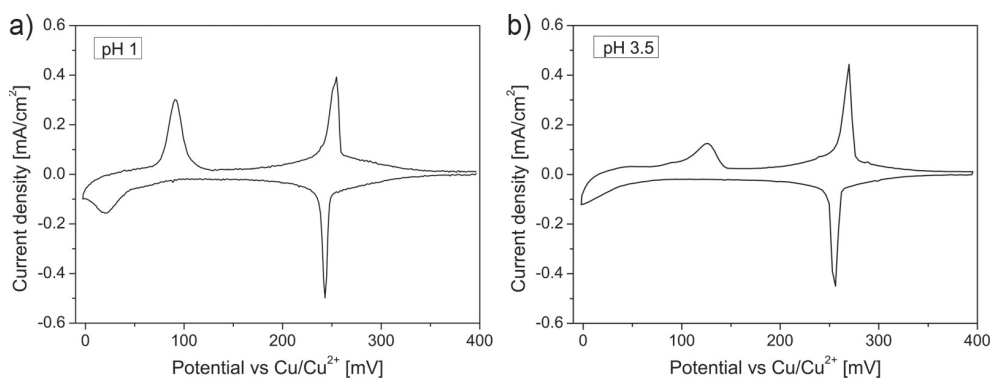


**Figure 3.2:** CV's of Cu UPD on Au(111) from sulfate solutions with different acidities. The CV in (a) was measured in 10 mM  $\text{CuSO}_4$  and 0.1 M  $\text{H}_2\text{SO}_4$  solution with a pH of 1, and (b) in 10 mM  $\text{CuSO}_4$  and 0.1 M  $\text{K}_2\text{SO}_4$  solution with a pH of 3.5. Potential sweep rate: 30 mV/s.

Figure 3.2a shows a CV of a Au(111) single crystal in a 10 mM  $\text{CuSO}_4$  and 0.1 M  $\text{H}_2\text{SO}_4$  solution (pH 1). The negative peak at 245 mV and the positive peak at 250 mV correspond to the formation and the dissolution of the  $(\sqrt{3} \times \sqrt{3})R30^\circ$  UPD

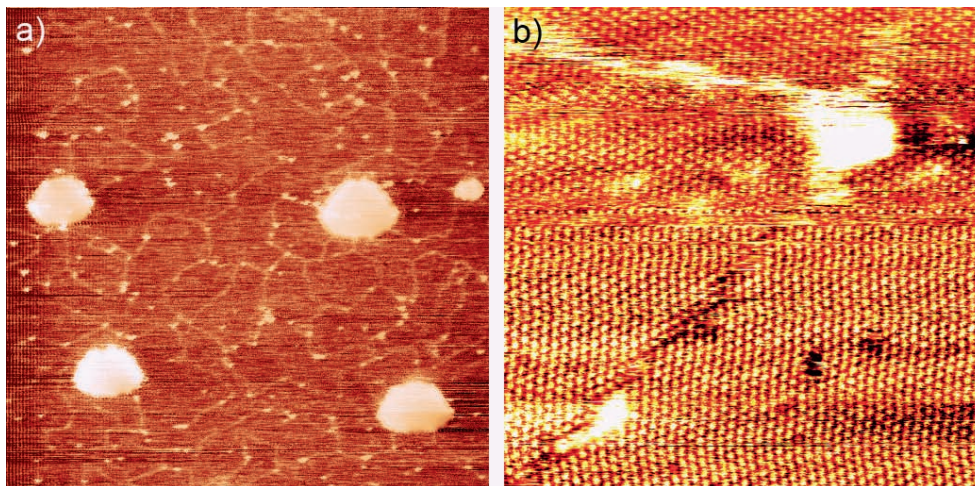
layer. These peaks will be further referred to as the *first UPD* deposition and dissolution peak correspondingly. The peaks found at more negative potentials ( $\sim 25$  mV and  $\sim 90$  mV) correspond to the transformation of the UPD layer from the  $(\sqrt{3} \times \sqrt{3}) R30^\circ$  to the  $(1 \times 1)$  structure and vice versa. These peaks will be referred to as the *second UPD* deposition and dissolution peaks. Integration of the two deposition current peaks gives a total charge density of  $480 \mu\text{C}/\text{cm}^2$  for the formation of the UPD layer. This value is in a good agreement with the value of  $460 \mu\text{C}/\text{cm}^2$  found in literature [23]. The CV changes significantly, if the acidity of the solution is decreased, as can be seen in the CV of a Au(111) single crystal in a 10 mM  $\text{CuSO}_4$  and 0.1 M  $\text{K}_2\text{SO}_4$  solution (pH 3.5), see Fig. 3.2b. The pair of the first UPD peaks is shifted by 15 mV to more positive potentials. The maximum of the second UPD deposition peak is no longer resolved as it overlaps with the current of the onset of the bulk deposition. The second UPD dissolution peak lies at a more positive potential than the corresponding peak in the pH=1 solution.

Figure 3.3a shows a large scale image of the Au(111) surface covered with the UPD layer. Note that the bright islands on the surface are islands with a monatomic step height of Au(111), which were also present before the Cu UPD layer formation. The UPD layer consists of domains with clearly visible domain boundaries. These domain boundaries may be interpreted as defects of the UPD layer, which indicates that the UPD layer in a sulfate electrolyte is rather defect-rich. After analyzing STM images with atomic resolution of different domains, we can conclude that there are three orientations of the domains, which reflects the three-fold symmetry of the Au(111) surface. As one can see in Fig. 3.3a, many domains have boundaries that are not related to the edges of the preexisting, large Au islands. This means that those domains must have nucleated on terrace sites and not at the edges of the preexisting Au islands. As we will see in Section 3.3.2, this contrasts our observations of the formation of the UPD layer from  $\text{Cl}^-$ -containing solution, where we have strong evidence for the nucleation of the UPD layer at step edges.

Figure 3.3b shows the Cu UPD with higher magnification: domain boundaries as well as "atoms" are visible. It has been shown that the "atoms" in the UPD layer observed with the STM correspond to the sulfate anions coadsorbed with Cu [102]. The nearest neighbor distance in this image is  $0.48 \pm 0.04$  nm, which corresponds well to the  $(\sqrt{3} \times \sqrt{3}) R30^\circ$  structure; the theoretical value of the nearest-neighbor distance for the  $(\sqrt{3} \times \sqrt{3}) R30^\circ$  structure on a Au(111) surface is  $\sqrt{3} \times 0.288$  nm = 0.499 nm.

It is interesting to mention that although the change of the pH from 1 to 3.5 leads to a significant change of the CV of the Cu UPD on Au(111), there is no pronounced change in the structure of the UPD layer derived from the STM images. With a pH of 3.5 the STM measurements reveal a  $(\sqrt{3} \times \sqrt{3}) R30^\circ$  structure with a nearest-neighbor distance of  $0.47 \pm 0.04$  nm. However, the structure that is formed during the second UPD deposition peak might differ from that of the initial UPD layer (an analysis has not

been performed within the framework of this thesis).

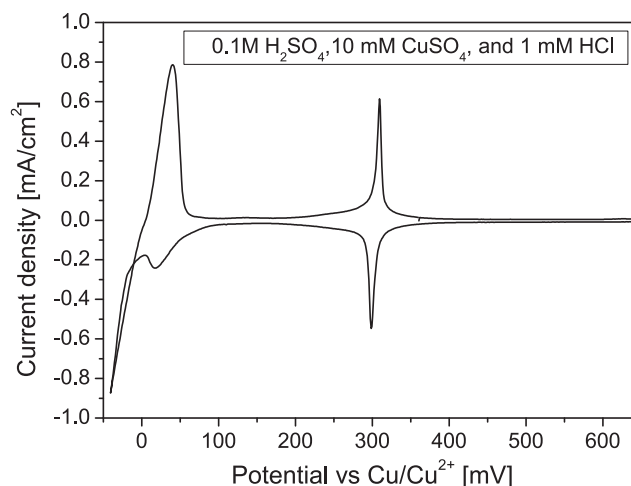


**Figure 3.3:** STM images of the Cu UPD layer formed in a 10 mM  $\text{CuSO}_4$  and 0.1 M  $\text{H}_2\text{SO}_4$  solution on a Au(111) single crystal surface. (a) The domain boundaries of the UPD layer are clearly visible. The height of the "large" islands in the image corresponds to a monatomic Au(111) step. The image scale is  $200 \times 200 \text{ nm}^2$ . (b) Higher magnification of the UPD layer with atomic resolution; the "atoms" are the coadsorbed sulfate anions. The scale is  $20 \times 20 \text{ nm}^2$ . The tunneling parameters are: 15 mV tip potential, 200 mV sample potential, and 500 pA tunneling current.

### 3.3.2 Effect of chloride on the Cu UPD

Addition of even small amounts of  $\text{Cl}^-$  to the solution changes both the CV and the structure observed with the STM. Figure 3.4 shows a CV of Cu deposition on Au(111) in the UPD regime from a solution with 0.1 M  $\text{H}_2\text{SO}_4$ , 10 mM  $\text{CuSO}_4$ , and 1 mM HCl. The CV shows two pairs of peaks, similar to the case of sulfate-containing but chloride-free electrolyte. The peaks at about 305 mV are reversible and appear at potentials that are more positive than in the case of sulfuric acid without  $\text{Cl}^-$ . The second pair of peaks overlaps somewhat with bulk Cu deposition (or dissolution), but the maximum of the second UPD deposition peak at 15 mV is well-separated. In fact, the second UPD stripping peak in the CV of Fig. 3.4 appears much larger than the corresponding deposition peak. The reason is that the second UPD stripping peak overlaps with the stripping peak of the bulk deposit that grew during the cathodic sweep below 0 mV. By integrating the two deposition peaks we find that the charge transferred during the formation of the UPD is  $350 \mu\text{C}/\text{cm}^2$ . This value corresponds well to the value of 360 mV

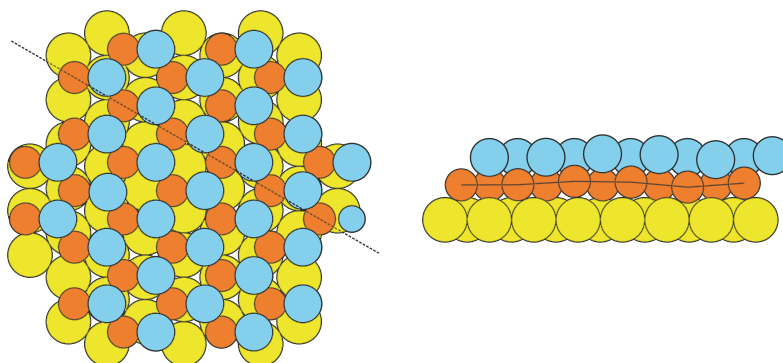
from the literature [103]. Note that the charge density estimate is only approximate due to the overlap of the second UPD deposition peak with the bulk copper deposition.



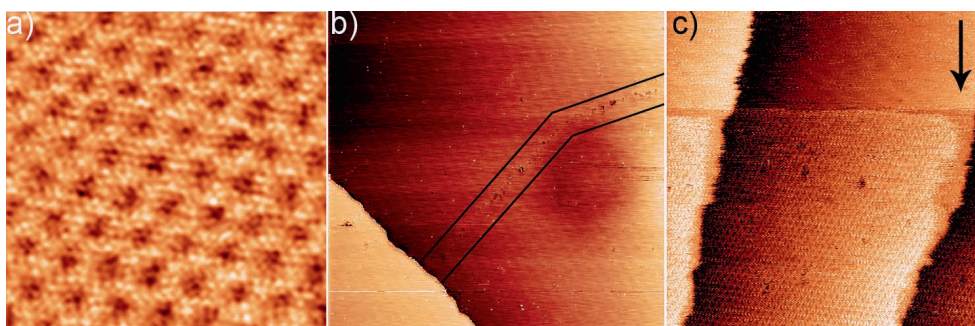
**Figure 3.4:** CV of Cu UPD on Au(111) in the presence of  $\text{Cl}^-$ . The solution contains 0.1 M  $\text{H}_2\text{SO}_4$ , 10 mM  $\text{CuSO}_4$ , and 1 mM HCl. The potential sweep rate is 30 mV/s.

Figure 3.5 shows a model of the Cu UPD layer in the presence of  $\text{Cl}^-$ . Using various techniques it was shown that during the UPD in  $\text{Cu}^{2+}$  and  $\text{Cl}^-$  containing solutions on Au(111) a bi-layer is formed, consisting of a bottom Cu layer and a top Cl layer [23]. Due to the lattice mismatch between the UPD layer and the Au(111) surface, the UPD layer shows a long-range modulation that reflects the moiré pattern between the two lattices. The moiré pattern implies that the atoms in the UPD layer are periodically displaced in the direction perpendicular to the surface. Also, it was demonstrated that the Cu atoms are packed in registry with the top layer of chloride, see Fig. 3.5, and not in registry with the underlying gold layer [104].

Figure 3.6a shows an atomically resolved STM image of the "(5 × 5)" structure of the UPD layer in  $\text{Cl}^-$ -containing electrolyte obtained at a potential of 260 mV, which is between the first and the second UPD deposition peaks. We measure the period of the moiré pattern to be  $1.31 \pm 0.05$  nm. Within the moiré pattern one can see a corrugation with a shorter period of  $0.37 \pm 0.03$  nm, corresponding to individual Cl atoms of the UPD layer. Figure 3.6b shows a  $200 \times 200$  nm<sup>2</sup> STM image of the Au(111) surface covered by the Cu UPD. Three domains are visible on the surface with one domain boundary corresponding to the monatomic step and another domain boundary on the flat terrace. If one compares Fig. 3.6b with Fig. 3.3a, one notices that the UPD layer in the  $\text{Cl}^-$ -containing electrolyte has much less defects as compared to the UPD layer grown in the sulfate containing electrolyte without  $\text{Cl}^-$ . The reason might be a greatly enhanced



**Figure 3.5:** Atomic ball model of the copper chloride bilayer that forms on top of Au(111). The yellow, orange, and blue balls correspond to gold, copper, and chloride atoms, respectively. Due to the lattice mismatch between the bilayer and the Au(111) surface, the adlayer is buckled. The image has been reproduced with permission from [101].



**Figure 3.6:** STM images of Cu UPD on Au(111) in the presence of  $\text{Cl}^-$ . The solution contains 0.1 M  $\text{H}_2\text{SO}_4$ , 10 mM  $\text{CuSO}_4$  and 1 mM  $\text{HCl}$ . (a) In the  $10 \times 10 \text{ nm}^2$  atomically resolved image, both the long-range moiré pattern and single Cl atoms are clearly visible. The image is low-pass filtered for clarity. (b) The  $200 \times 200 \text{ nm}^2$  image shows a UPD layer with much less defects, exhibiting only three domains. One domain boundary follows the atomic step and the other one, on the lower terrace, runs between the two black lines. (c) The  $65 \times 65 \text{ nm}^2$  image shows the formation of the UPD layer. The image is taken during a potential sweep from 305 mV to 297 mV at 0.1 mV/s. The arrow represents the time axis. Note that the UPD layer has "difficulties" in covering the whole terrace: the vicinity of the step at the higher terrace side remains uncovered although, the area decreases with decreasing sample potential. The tunneling parameters are: 0 mV tip potential, and 1 nA tunneling current. In (a) and (b) sample potential was 260 mV.

Cu mobility in the presence of  $\text{Cl}^-$ , which is also suggested in literature [105, 106]. Due to a higher Cu mobility, the capture zones for Cu adatoms around UPD layer nuclei are much larger than in the  $\text{Cl}^-$ -free solution, resulting in a smaller density of larger domains

and hence less domain boundaries.

Figure 3.6c shows an STM image of the Cu UPD layer formation process during a potential sweep from 305 mV to 297 mV. The particular shape of the UPD layer growth front strongly suggests that the UPD layer nucleates at the steps, similar to the process reported in [107]. During the potential sweep to more negative values over the UPD peak, the Cu UPD layer rapidly covers almost the complete terraces, but leaves the vicinity of each step on the higher-terrace side uncovered, see Fig. 3.6c. Further change of the potential to slightly more negative values is needed to fill up the terraces completely. This growth behavior can be explained by step-step interactions [106]. In particular, the Smoluchowski-effect leads to a local variation of the surface potential at the steps [108]. Also, entropic step-step repulsion could contribute to the observed effect [109]. We expect this observation to be a general effect that might take place on a variety of different systems during a UPD layer formation. In measurements where some contamination was present on the terraces of the surface, as observed by the STM, nucleation of the UPD layer occurred also on the terraces.

Surprisingly, the structure of the Cu UPD layer at potentials around the second UPD peak, as well as at more negative potentials, remains unknown. The "(5 × 5)" structure is visible at these potentials in the STM measurements, as reported in literature [107] as well as observed in our experiments. However, we see that the contrast of the moiré pattern changes at the second UPD peak. On the basis of our STM images, we are unable to ascribe the observed change of the contrast to a change in the layer structure. More measurements are needed to clarify this issue.

## 3.4 Effect of SPS on Cu UPD

### 3.4.1 SPS and Cu underpotential deposition with Cl<sup>-</sup>

Figure 3.7 shows a comparison between CV's in SPS-free and SPS-containing solutions. The SPS-free solution is the same as used in Fig. 3.4. The SPS-containing solution is prepared by adding 10 μM SPS to the SPS-free solution. In the presence of SPS the center of the first Cu UPD deposition peak is shifted by 70 mV to more negative values as compared to SPS-free solution, showing that SPS makes the Cu UPD more difficult. In addition, the peak shape suggests that it consists of two overlapping single peaks, see "I" and "II" in Fig. 3.7. The charge density associated with the UPD peak in the SPS-containing electrolyte equals 340 μC/cm<sup>2</sup>, as is estimated by integrating the current peak in the CV. As it was noted in Section 3.3.2, the total charge density associated with the first Cu UPD in SPS-free electrolyte amounts to 350 μC/cm<sup>2</sup>, which agrees well with the charge density of the Cu UPD layer formation in SPS-containing solution. However, we argue that the agreement between the charges of UPD layer formation

with and without SPS is accidental, since the structure of the Cu UPD layer is different in both cases. In fact, our EC-STM measurements of SPS adsorption on a Cu UPD layer that is preformed in a SPS-free electrolyte, indicate that the structure of the UPD layer is changed dramatically after exposure to the SPS, see Section 3.6.1. Note also that in the SPS-containing solution there is no second UPD peak as in the SPS-free solution. This lets us assume that the Cu UPD process is completed at more positive potentials than the second UPD deposition peak in the SPS-free solution (15 mV) but more negative than the first UPD deposition peak in the SPS-containing solution (235 mV). In addition this also implies that the structure of the UPD deposit remains unchanged (in contrast to the SPS-free case) until the onset of the bulk deposition.

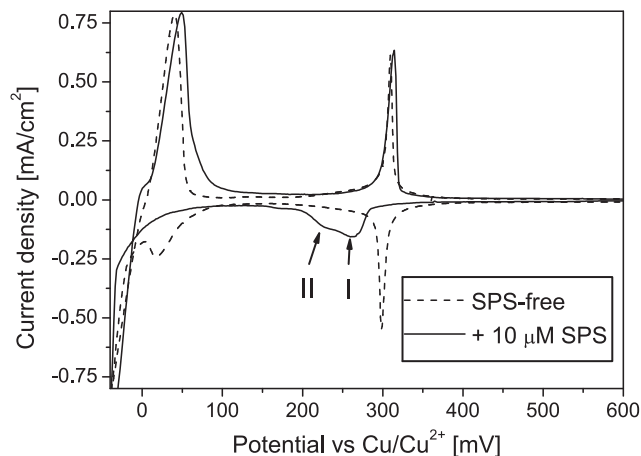


**Figure 3.7:** Cyclic voltammograms comparing Cu UPD on Au(111) in a solution containing 0.1 M  $\text{H}_2\text{SO}_4$ , 10 mM  $\text{CuSO}_4$ , and 1 mM HCl, with (solid line) and without (dashed line) 10  $\mu\text{M}$  SPS. Note that the CV in the SPS-containing electrolyte has been recorded several minutes after SPS addition to the solution. The voltage sweep rate is 30 mV/s. Note also the two distinct peaks "I" and "II" of the UPD deposition in SPS-containing electrolyte.

Although the first UPD deposition peak strongly deviates in the SPS-containing solution, the position of the first UPD stripping peak remains, surprisingly, almost unchanged in the case of the SPS-containing electrolyte. Based on this information one could guess that SPS is not strongly incorporated in the Cu UPD layer upon its formation. The shape of the stripping peak becomes less symmetric in the presence of SPS, as compared to the SPS-free case: it shows a slower starting of the stripping and a faster finish.

The height and the shape of the UPD current peaks "I" and "II" in the SPS-containing electrolyte, are significantly changed, if the potential of the sample is kept for several tens of minutes at a value around 710 mV, *i.e.* higher than the UPD layer formation and lower than the Au(111) monolayer oxidation potential of 1030 mV, see Fig. 3.8. With

increasing waiting time at 710 mV, the height of peak "I", located at 265 mV, decreases. The peak also becomes wider. Peak "II", found at 210 mV, becomes more pronounced, as its height increases. The total charge density of the UPD layer formation remains almost unchanged; it is equal within  $15 \mu\text{C}/\text{cm}^2$ . Raising the sample potential above the gold monolayer oxidation potential restores the original shape of the UPD peaks, as depicted by the dashed line in Fig. 3.8. We believe that, when waiting at 710 mV, the change is caused by additional adsorption of SPS molecules on the Au(111) surface and an increase of the SAM quality, *i.e.* increase of the SAM domain size. In fact, a change of the CV due to thiol adsorption at similar timescales has been observed in Ref. [88]. Also, it has been shown in Ref. [94] that the adsorption and ordering of SPS on Au(111) proceeds at a comparable time scale as our waiting time. If the potential is changed to more positive values, *i.e.* around the gold oxidation potential, the SPS molecules are oxidatively desorbed from the surface [110]. Oxidation of the SPS can be associated with the increase of the oxidative current in the CV in the potential range between 800 mV and 1000 mV, see Fig. 3.8. Thus, the subsequent CV sweep would result in a similar curve as in the case of a surface that is freshly exposed to the SPS-containing electrolyte. However, we have to note that we cannot rule out the possibility of the presence of contaminants, that could also lead to the change of the UPD layer formation peaks.

Please note that the shape of the CV's in the SPS-containing electrolyte was quite reproducible in our experiments upon subsequent cycling in the potential range of 10 mV to 900 mV, as opposed to several other studies [75, 78], where some damage of the SAM has been observed.

Figure 3.9a shows an STM image of the Au(111) surface exposed to the SPS-containing electrolyte. While taking the image, the sample potential was swept from 265 mV to 210 mV, thus covering the potential range of the Cu UPD layer formation. As compared to Sections 3.3.1 and 3.3.2, the Cu UPD layer formation process is strongly influenced by the presence of the SPS. We do not see the nucleation of the Cu UPD layer at the step edges and rapid covering of complete terraces, as observed in the SPS-free electrolyte, see for comparison Fig. 3.9. Instead, the UPD layer formation proceeds in two steps. Firstly, in the potential range between 270 mV and 230 mV patch-like structures nucleate everywhere on the surface and grow out towards more negative potentials, reaching surface coverage of around 80%. Secondly, at potentials below 230 mV islands nucleate that are higher than the patches. These islands grow out slightly, reaching the maximum surface coverage of 9%. In the following we discuss the different steps of the Cu UPD layer growth in the SPS-containing solution in more detail.

Figure 3.9b shows a typical STM image of the Au(111) surface in an electrolyte at potentials more positive than the Cu UPD layer formation potential (310 mV to 610 mV)

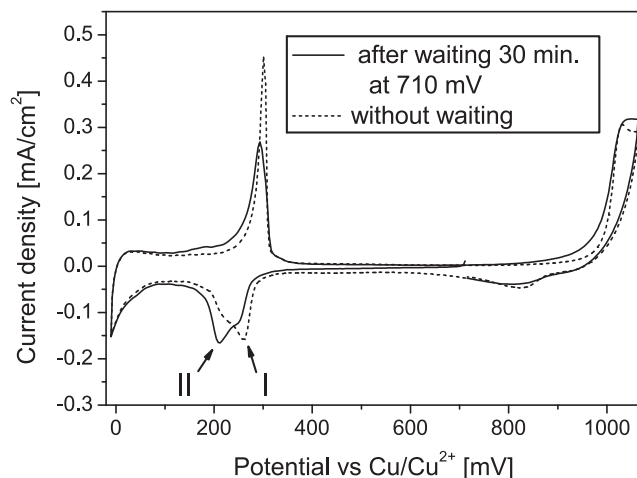


**Figure 3.8:** Two subsequent cyclic voltammograms of Au(111) in 0.1 M H<sub>2</sub>SO<sub>4</sub>/10 mM CuSO<sub>4</sub>/1 mM HCl/10 μM SPS. The solid curve has been measured after the sample potential was kept at 710 mV for 30 minutes. The potential has been swept in the cathodic direction; thus the UPD peaks of the solid curve are measured before the surface was oxidized. The dashed curve corresponds to the subsequent scan after surface oxidation (at 1030 mV) and reduction (peak at 820 mV). The voltage sweep rate is 30 mV/s. Note the peak height changes of "I" and "II" in the different cases.

after introduction of SPS into the liquid cell. Monatomically deep holes, characteristic for thiol adsorption [72–74], are formed after several tens of seconds after introduction of 10 μM SPS. The coverage of the vacancy islands ranges from 2% to 9% of a monolayer. The entire surface is covered with domains of ordered, self-assembled structures of SPS, or MPS (monomer of SPS), as argued in [94]. According to the crystal symmetry, three orientations of the domains are visible. In fact, the molecularly resolved structure of the SAM (see Fig. 4.3 in Chapter 4) strongly resembles measurements on a SAM of MPS by Ref. [94] in Cu<sup>2+</sup>-free and Cl<sup>-</sup>-free electrolyte. Thus, we can assume that the SAM observed in our measurements probably consists of MPS molecules, which were created due to the sulfur-sulfur bond cleaving of the SPS molecules upon adsorption at the substrate. We further mention that at these potentials no Cu is present at the surface.

If the potential is changed to 250 mV, *i.e.* the potential where peak "I" of the double UPD peak is found, small islands of deposit (called "UPD patches" further in the text) appear on the terraces, see Fig. 3.9c. These patches do not nucleate preferably at Au steps or surface defects, as in the case of the additive-free solution. Instead, they are formed homogeneously on the terraces. Closer inspection indicates that these patches prefer to nucleate at the defects of the SAM, *i.e.* at the domain boundaries between

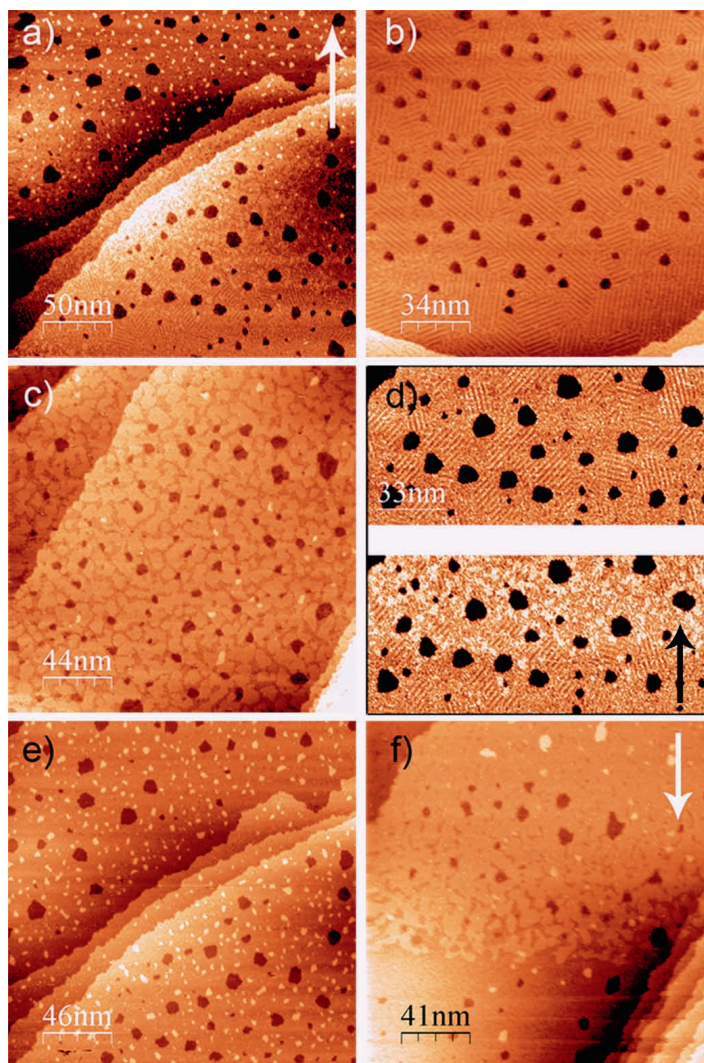


**Figure 3.9:** STM images of the Cu UPD layer growth in solution containing 0.1 M  $\text{H}_2\text{SO}_4$ , 10 mM  $\text{CuSO}_4$ , 1 mM  $\text{HCl}$ , and 10  $\mu\text{M}$  SPS. The arrow shows the scan and the sample potential sweep direction. (a) Different stages of the Cu UPD layer formation during a potential sweep from 265 mV to 210 mV. (b) The surface is covered by a SAM of SPS. The sample was exposed to SPS-containing solution for 25 minutes at a potential of 360 mV. (c) UPD patches at the surface at 250 mV. (d) Two consecutive images of the same surface area, showing the nucleation of the UPD patches. The upper image was acquired at a potential of 310 mV. In the lower image the potential was swept from 265 mV to 250 mV. (e) Islands with a height of a monatomic step on Au(111) (higher than the patches) that nucleated between the UPD patches at 170 mV. (f) UPD layer stripping: the potential was swept from 250 mV to 310 mV. All images were acquired at tip potentials between 10 mV and 90 mV and tunneling currents between 150 pA and 500 pA.

SAM areas of different orientations, see Fig. 3.9d. Such growth behavior has also been observed in other studies [91]. However, this effect is much less obvious in our case due to the high defect density, *i.e.* small domain size, and low packing density of the SAM. The height of the patches as measured with STM is  $0.10 \pm 0.03$  nm. This matches well with the height of the Cu UPD layer grown in the absence of SPS. Also, these patches do not appear in the solution without  $\text{Cu}^{2+}$  ions. We conclude that these patches are copper underpotential deposit.

Upon further lowering of the potential the UPD patches coalesce and at the potential of peak "II" of the double UPD peak (210 mV) small islands that are higher than the UPD patches appear on the terraces, see around the middle (and slightly above the middle) of Fig. 3.9a as well as Fig. 3.9e. These islands nucleate in between the patches, *i.e.* on the parts of the surface that are not covered by the UPD layer. The height of the islands is  $0.24 \pm 0.02$  nm, which matches well with the height of a monatomic Au(111) step of 0.235 nm. The island coverage ranges between 1 – 9% of a monolayer. We attribute this spread to different SPS surface coverage at the beginning of the UPD layer formation, see Fig. 3.8 as well as further in the text.

The stripping of the UPD layer happens in a single step, as opposed to the two-step UPD layer growth process. The UPD copper layer rapidly breaks down into patches, which then quickly disappear together with the islands, see Fig. 3.9f. Some of the larger islands remain stable over some time, even if there is no UPD layer present anymore.

We would like to mention here that the fraction of the surface covered by the UPD patches, see Fig. 3.9c, depends not only on the potential but also on time, see Fig. 3.10.

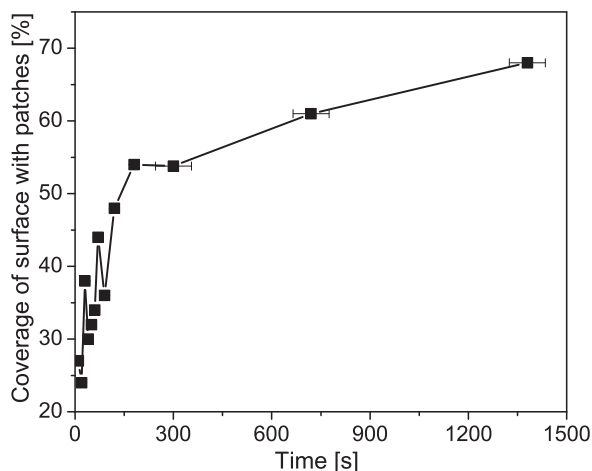


**Figure 3.10:** Fraction of the surface covered by UPD patches as a function of time after the potential was lowered from 340 mV to 235 mV. The non-zero starting coverage reflects the finite duration of the change of potential to 235 mV.

### 3.4.2 Cu UPD from a Cl<sup>-</sup>-free solution in presence of SPS

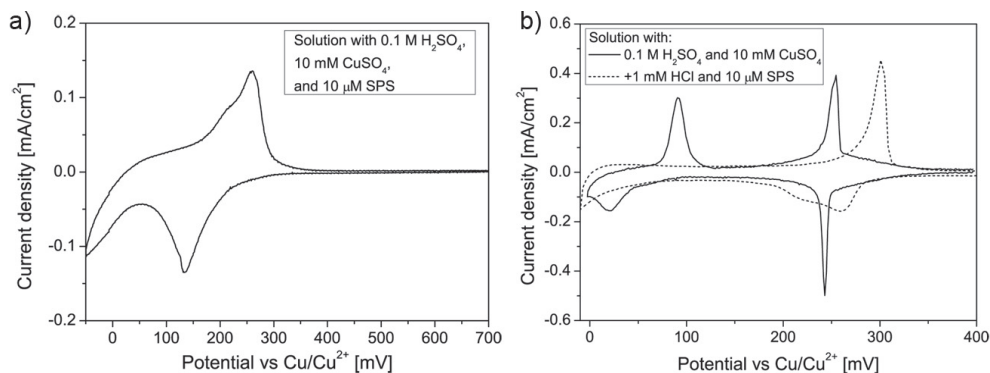
To probe the effect of Cl<sup>-</sup> on the Cu UPD in the presence of SPS, we have repeated the experiments in an electrolyte containing sulfate but no chloride. The reason for repeating experiments in the Cl<sup>-</sup>-free electrolyte is that the Cl<sup>-</sup> ions might have a significant influence on the observed processes. For example, it is reported in literature [1, 111] that the concentration ratio between SPS and Cl<sup>-</sup> affects the Cu bulk deposition.

Figure 3.11a shows the CV of Au(111) in a solution, containing 0.1 M H<sub>2</sub>SO<sub>4</sub>, 10 mM CuSO<sub>4</sub>, and 10 μM SPS. Only one pair of peaks corresponding to the Cu UPD layer formation is visible, unlike in the SPS-free solution, where the UPD layer formation resulted in two separate pairs of peaks, see Fig. 3.2a. Similar to the Cl<sup>-</sup>-containing electrolyte (Fig. 3.7), the Cu UPD growth peak is shifted to more negative potentials in the presence of SPS, compare Figs. 3.11a and b (solid line). The peak is much broader than in the SPS-free solution, suggesting that the presence of the SPS hinders the UPD layer formation. However, it is not clear from the peak shape, whether the UPD layer formation happens in one or several steps, i.e. there are no obvious overlapping peaks within the broad peak as in Figs. 3.11b (dashed line) and 3.7. The position of the current maximum of the Cu UPD stripping peak is at 260 mV; it is almost unchanged by the presence of SPS. However, the peak is much broader as compared to the SPS-free electrolyte and its maximum is much less sharp. The shoulder in the peak at 220 mV indicates that the peak is made of two overlapping peaks. The charge density associated with the Cu UPD layer formation in the Cl<sup>-</sup>-free but SPS containing electrolyte is 375 μC/cm<sup>2</sup>. This value is 100 μC/cm<sup>2</sup> smaller than in the SPS-free electrolyte. It is however compatible with the charge density of the Cu UPD layer formation in solution with Cl<sup>-</sup> and SPS, suggesting that the final structure of the layer could be determined by the SPS rather than by the anions, see also Section 3.6.1.

Comparing the CV's in Fig. 3.11a and Fig. 3.11b (dashed line), we can draw the following conclusions. Firstly, the type of the dominating anion in the solution, i.e. either Cl<sup>-</sup> or SO<sub>4</sub><sup>2-</sup>, changes the Cu UPD deposition peak. Thus, we can assume that the anions are co-adsorbed during the Cu UPD layer formation in SPS-containing electrolyte, much like in the SPS-free solution<sup>1</sup>. Secondly, the SPS is also co-adsorbed during the Cu UPD layer growth. This becomes especially obvious from the UPD stripping peak in Cl<sup>-</sup>-free electrolyte with SPS, which is changed dramatically with respect to the same peak in the SPS-free electrolyte.

Figure 3.12 shows STM images of the Au(111) in the Cl<sup>-</sup>-free but SPS-containing electrolyte. The Au(111) surface at the surface potential of 230 mV exhibits domains of the ordered SAM of SPS, see Fig. 3.12a. We found no difference in the structure

<sup>1</sup> It has been shown that although anions are present on the Au(111) surface at more positive potentials than the Cu UPD layer formation potential, during the Cu UPD process additional anions are co-adsorbed together with the Cu<sup>2+</sup> cations [23, 103, 104, 112].



**Figure 3.11:** CV of Au(111) in the UPD potential region (a) in a solution containing 0.1 M  $\text{H}_2\text{SO}_4$ , 10 mM  $\text{CuSO}_4$ , and 10  $\mu\text{M}$  SPS. Note that the curving of the CV towards negative currents in the potential range between 0 mV and 50 mV is due to the presence of oxygen in the solution, leading to oxygen reduction. (b) The CV's in the solution containing 0.1 M  $\text{H}_2\text{SO}_4$ , 10 mM  $\text{CuSO}_4$  (solid line) and with additional 1 mM  $\text{Cl}^-$  and 10  $\mu\text{M}$  SPS (dashed line) are shown for comparison.

of the SAM as compared to the  $\text{Cl}^-$ -containing solution, see Fig. 3.9b. Also, as in the  $\text{Cl}^-$ -containing electrolyte at these potentials, vacancy islands are present on the surface. As the potential is lowered, first a disordered phase is observed in the potential range from 210 mV to  $\sim 185$  mV, see Fig. 3.12b and c. Within the disordered phase small patches can be distinguished. However, these patches are not as well-defined as the patches observed in the  $\text{Cl}^-$ -containing solution, compare inset in Fig. 3.12c with Fig. 3.9c. At  $\sim 195$  mV islands start to appear at the surface, similar to the islands observed in the  $\text{Cl}^-$ -containing electrolyte. The height of these islands is  $0.241 \pm 0.065$  nm, comparable to the height of the islands in the the  $\text{Cl}^-$ -containing electrolyte. The islands remain stable in potential region where the Cu UPD layer is present on the surface, see Fig. 3.9d.

Based on these observations, we conclude that the surface morphology of the formed Cu UPD is not influenced by either presence or absence of  $\text{Cl}^-$  in the solution. There is however a clear difference in the initial stage of the Cu UPD layer formation: rather stable patches of the Cu deposit are formed with  $\text{Cl}^-$  in the solution, whereas without  $\text{Cl}^-$  a more dynamic and disordered phase is observed. This difference between the  $\text{Cl}^-$ -free and  $\text{Cl}^-$ -containing electrolytes with SPS can be understood if one considers the interaction strength between the copper and  $\text{Cl}^-$ ,  $\text{SO}_4^{2-}$ , and SPS. It is generally known that  $\text{Cl}^-$  adsorbs more strongly than  $\text{Cl}^-$  on bulk Cu(111), Au(111), and on the Cu UPD layer on Au(111) [113, 114]. Thus, for example, in Ref. [115] it has been shown that addition of only  $5 \times 10^{-6}$  M NaCl to a 0.05 M  $\text{H}_2\text{SO}_4$  electrolyte containing 1 mM  $\text{CuSO}_4$  changed both the CV as well as the atomic structure of the Cu UPD layer, indi-

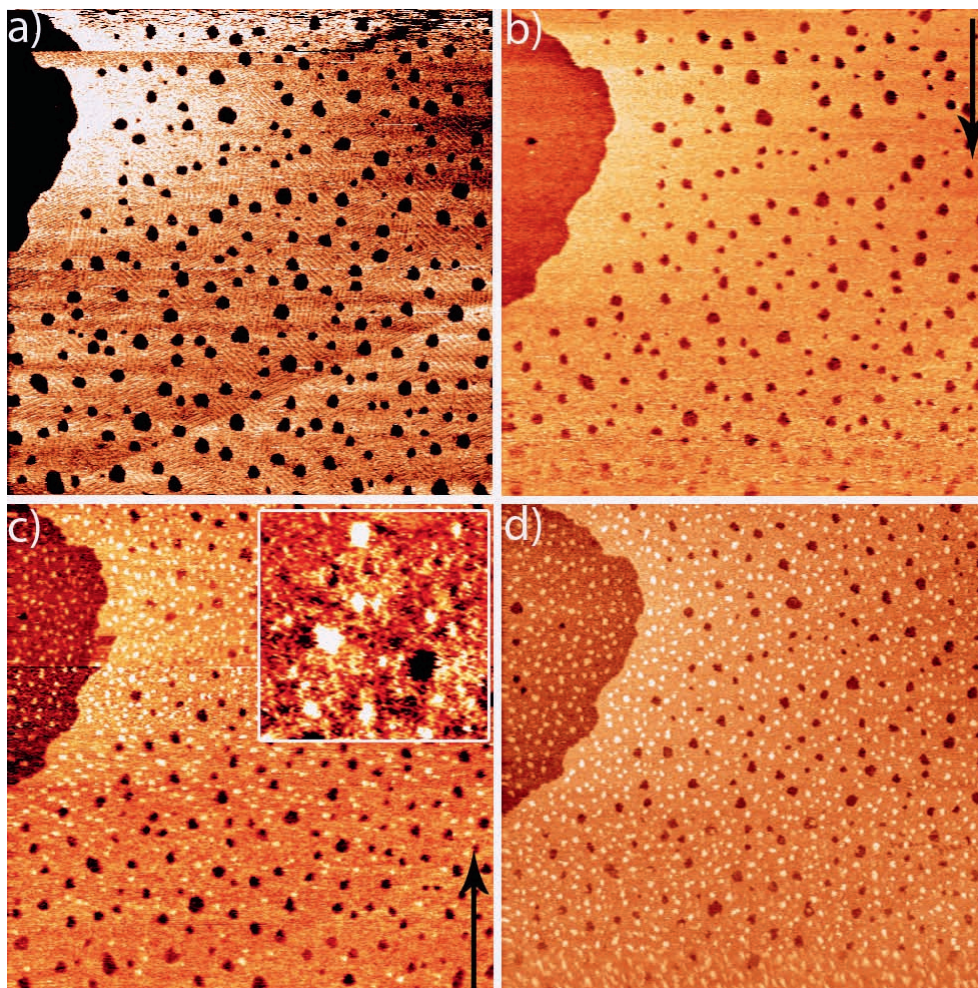


**Figure 3.12:** STM images of Cu UPD on Au(111) in a Cl-free electrolyte with SPS. The electrolyte composition is 0.1 M  $\text{H}_2\text{SO}_4$ , 10 mM  $\text{CuSO}_4$ , and 10  $\mu\text{M}$  SPS. (a) The surface is covered by ordered domains of the SAM. Also monatomically deep vacancy islands (corresponding to a Au(111)-step height) are visible. The surface potential is 230 mV. In (b) and (c) the potential was swept from 230 mV to 200 mV in (a) and from 200 mV to 170 mV in (b) at a rate of 0.5 mV/s. Around the center of (b) (at  $\sim 215$  mV) small patches nucleate in between the disordered phase on the surface. The patches are not as well-defined as in Fig. 3.9c. In (c) islands with a height of a monatomic step on Au(111) appear. The arrows in the images indicate the time axis of the sweep and the scan direction. The inset shows a  $30 \times 30 \text{ nm}^2$  zoom-in image at 190 mV, showing the islands (white spots), Au vacancy island (black spot), and the disordered phase with small patches. (d) shows the surface after the completed Cu UPD layer formation at the surface potential of 160 mV. The islands with a height of a monatomic step of Au(111) are visible on the terraces. The size of images (a)-(d) is  $200 \times 200 \text{ nm}^2$ . The tunneling parameters are: 100 mV tip potential, 300 pA tunneling current.

cating a much stronger affinity of  $\text{Cl}^-$  to the Cu UPD layer than that of sulfate. On the other hand, the affinity of a thiol, such as a simple alkane-thiol or SPS, to a Cu surface is somewhat higher than that of  $\text{Cl}^-$ : for example, the binding energy of a methanethiol to a Cu(111) surface was calculated to be 2.08 eV per molecule [116], whereas for  $\text{Cl}^-$  a value of 1.89 eV was obtained [117]. Although the above values were obtained for a single-crystal Cu(111) surface, we expect the tendency to be the same for the binding to the Cu UPD layer on Au(111). Thus, we propose the following explanation to our experimental observations. At the onset of Cu UPD, Cu is co-deposited together with the anions, and probably also with the SPS from the solution. In the absence of  $\text{Cl}^-$ , Cu is deposited together with sulfate and SPS. Since the thiol-copper interaction is much stronger than the interaction of sulfate-copper, there will be a large amount of SPS incorporated in the UPD and also the diffusion of the SPS molecules from the Au surface to the UPD deposit will be largely unhindered, since the displacement of the sulfate molecules on the Cu UPD layer by SPS is energetically favorable. This could lead to the dynamic appearing patches observed in our STM measurements. In contrast, if  $\text{Cl}^-$  is present in the electrolyte, it will be the dominant anion species coadsorbed with Cu. Probably, SPS will also be coadsorbed, but in smaller amounts than in the absence of Cl, since the binding energy of a thiol to Cu is only slightly larger than that of  $\text{Cl}^-$ . Also, there will be a much higher energy barrier for the thiol molecules present on the Au surface to diffuse onto the growing Cu deposit due to a small difference between the binding energies of SPS/Cu and  $\text{Cl}^-/\text{Cu}$ . This could explain why we observe rather stable Cu UPD patches in the initial stage of Cu UPD in  $\text{Cl}^-$ -containing electrolyte. We would like to mention already here that we come to a similar conclusion on the basis of STM measurements of SPS adsorption on a pre-grown Cu UPD layer that is formed in a SPS-free electrolyte either with or without  $\text{Cl}^-$ , see Section 3.6.1.

## 3.5 Model for UPD layer growth in the presence of SPS

### 3.5.1 Formulation of the model

Based on our observations, we propose the following model for the UPD layer growth in the presence of SPS or other thiol molecules [118]. As a starting situation we assume an unreconstructed gold surface, which is exposed under potentiostatic control to an electrolyte containing  $\text{Cu}^{2+}$  and  $\text{Cl}^-$  ions as well as the SPS molecules, see Fig. 3.13a. Please note that, although we assume that the electrolyte contains  $\text{Cl}^-$ , this model is also valid for a  $\text{Cl}^-$ -free solution with sulfate, as will be discussed below. At potentials, more positive than the UPD layer formation potential, but more negative than Au oxidation, SPS adsorbs at the surface [94], see Fig. 3.9b. As suggested already by other groups [6, 7, 70], we assume that the bond between each thiol molecule and the gold surface

is mediated by a gold adatom: when an SPS molecule is adsorbed, it extracts a gold atom from the surface, thus creating a surface vacancy. Due to the fast surface diffusion of single gold vacancies at room temperature [119, 120], the surface vacancies rapidly cluster [121]. Thus we expect the formation of a self-assembled SPS monolayer, which

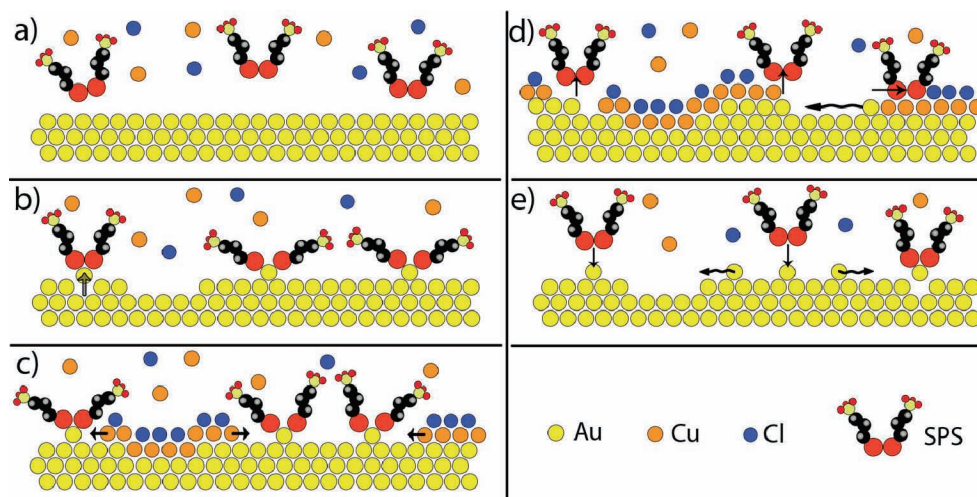


**Figure 3.13:** Model of the Cu UPD layer growth and stripping in the presence of SPS. (a) Initial situation of the surface exposed to the solution. (b) SPS adsorption on the surface mediated by gold adatoms, leading to the creation of vacancy islands. (c) Initial stage of the Cu UPD layer growth on the SPS-covered surface, resulting in the formation of Cu UPD patches. (d) Further growth of the Cu UPD patches, which forces the SPS molecules to release the gold atoms. This leads to the formation of gold islands, which in turn get covered by the Cu UPD layer. The Cu UPD exhibits islands with a step height of a Au(111) step. (e) Gold surface after stripping of the UPD layer; the gold islands disappear due to gold atom diffusion as well as re-adsorption of SPS. Re-adsorption of SPS also leads to formation of new vacancy islands. We did not consider the possible splitting of the SPS molecules to MPS molecules upon adsorption. This, however, does not influence the main conclusions of our model.

is accompanied by the formation of surface vacancy islands, see Fig. 3.13b. This is indeed the case, as can be seen in Fig. 3.9b. Also, vacancy islands are commonly observed as a result of thiol adsorption [72–74]. As we change the sample potential to more cathodic values, adsorption and reduction of Cu at the surface starts, leading to the formation of a Cu UPD layer. We observe that the UPD layer nucleates at the SAM defects, see Fig. 3.9b, from where it grows out, thereby squeezing the thiol molecules together. These molecules stay adsorbed on the gold surface and thus prevent the UPD layer from covering the whole surface, see Fig. 3.13c. We propose that this is the reason for the formation the UPD layer in patches. At a certain potential, when the UPD

coverage reaches a critical value, the thiol molecules are squeezed together so much that the repulsive interaction between them exceeds their binding energy to the gold. As a result, thiol molecules leave the gold surface and diffuse either into the electrolyte or onto the neighboring Cu UPD patches, see Fig. 3.13d. In this process they leave behind their gold atoms. Those gold adatoms, in turn, diffuse in the UPD-free regions of the surface and form small islands. These islands are then immediately covered by a copper UPD layer that stabilizes them against further diffusion, see Fig. 3.13d and Fig. 3.9e. Since the area around the islands as well as the islands themselves are covered by a Cu UPD layer, the apparent height of the islands, as measured with the STM, precisely equals the height of a Au(111) step. From now on, we refer to these Cu UPD islands as islands with a height of a monatomic Au(111) step. If, at this stage, the potential is increased to more anodic values, the Cu UPD layer is stripped, uncovering the gold surface, see Fig. 3.9f and 3.13e. The smaller gold islands rapidly disappear due to the high surface mobility of gold at room temperature, whereas the larger ones can remain present for some time, as observed experimentally, see Fig. 3.9f. Also, SPS molecules re-adsorb on the gold surface, again claiming gold adatoms, which could, in addition, be partly responsible for the annihilation of small gold islands and should also lead to the creation of new vacancy islands, see Fig. 3.13(e). This is again consistent with experimental observations.

The proposed model explains also well the double peak in the CV of the Cu UPD in the presence of SPS in the  $\text{Cl}^-$ -containing solution, as well as its waiting time dependence that is related to the SPS coverage, see Fig. 3.8. Based on the STM measurements, peak "I" of the UPD layer formation is attributed to the Cu UPD patch formation. At the moment when the thiol molecules are forced to leave the gold adatoms by the growing Cu UPD patches, SPS-free gold islands are created that are immediately covered by the Cu UPD layer, thus resulting in peak "II". We would expect the ratio between the two peaks to change, depending on both the thiol coverage on the surface prior to the UPD layer formation and on the domain size of the SAM. If the SPS coverage is low, the SAM would exhibit a large number of defects, such as *e.g.* domain boundaries. This would allow the UPD patches to nucleate and grow easily, leading to a sharp and well-pronounced peak "I". Higher coverage would lead to a better quality SAM. In this case the UPD patch nucleation and growth would be hindered more, as compared to lower SPS surface coverage, leading to a broader and smaller peak "I". The amount of gold released by SPS, *i.e.* the surface area of the gold islands, created in the second stage of the UPD layer formation, would also be dependent on the SPS coverage. Higher surface coverage would lead to a larger area of gold islands on the surface and to a larger peak "II" in the CV.

The above is exactly what we observe experimentally, see Figs. 3.7 and 3.8. The CV of the gold surface that has been exposed for a short time to SPS-containing solution

shows a higher peak "I" and a much smaller peak "II". When the surface is kept for some time at potentials around 710 mV, the SPS surface coverage and the SAM quality increase. This leads to a decrease in height and broadening of peak "I" as well as increase in height of peak "II".

It is tempting to quantify the adatom-mediated binding of the thiols to the Au surface in more detail. In general, one can distinguish two different cases [6, 7]. We define a dithiol linkage as the binding of one SPS (or two MPS) to *one* Au adatom, and a monothiol linkage as the binding of two MPS (or one SPS) to *two* Au adatoms. In order to receive more information on the type of linkage, one can compare the amount of adsorbed SPS molecules with the surface area of either the vacancy islands or the gold islands that emerge during the Cu UPD growth. The percentage of the surface occupied by the vacancy islands after the adsorption of the SPS molecules equals  $6\% \pm 2.6\%$ , as estimated from several experiments. The gold islands after the growth of the Cu UPD layer occupy  $5\% \pm 2.9\%$  of a monolayer. We attribute this large spread to active mono-vacancy and Au adatom diffusion and the existence of steps that are sources and sinks for both species. The specific conditions of SPS adsorption might also play a role, changing the balance between the rate of mono-vacancy creation, the time for diffusion, and the size of the vacancy islands. The coverage of the surface by the SPS molecules is hard to estimate from our experiments. As one can see in Figs. 3.9b and 3.9d, the surface is covered by a large number of small ordered domains of the thiols, separated by disordered regions. The area occupied by one SPS molecule (or two MPS molecules) in these domains is approximately  $2.7 \text{ nm}^2$ . If we would assume that the whole surface is covered by a single ordered domain of SPS, 3.5% of the surface Au atoms would be incorporated as adatoms in the SAM in the case of a dithiol linkage and 7% in the case of monothiol linkage. Comparing these values with both the vacancy and the island coverage, we are unable to distinguish between monothiol or dithiol linkage.

So far, in the description of our model, we have assumed the presence of  $\text{Cl}^-$  in the electrolyte. However, as we have mentioned above, the model can be applied without major modifications to the case of the  $\text{Cl}^-$ -free solution, as we observe the same general Cu UPD layer growth behavior in experiments with and without  $\text{Cl}^-$ , compare Fig. 3.9 with Fig. 3.12. Similar to the  $\text{Cl}^-$ -containing case, the Cu UPD layer growth proceeds in two distinct steps in the solution without  $\text{Cl}^-$ : first, patches of the UPD deposit appear and grow out, which is followed by the growth of islands with a Au(111) step height, see Fig. 3.12. However, the stages of the Cu UPD layer growth that are shown in Fig. 3.13c and d occur not consecutively, as in the case with  $\text{Cl}^-$ , but rather simultaneously. Thus, as the patches of the Cu deposit start to grow, the SPS molecules that are bound to gold atoms, can diffuse onto the patches and, probably, from the patches to the Au surface. The latter is possible since the binding energy of thiols to Au(111) is  $1.64 - 2.3 \text{ eV}$  [122], which is comparable to  $2.08 \text{ eV}$  for a thiol-Cu(111) bond [116]. We attribute the lower

stability of the patches and a possible lower diffusion barrier for the SPS to the lower affinity of  $\text{SO}_4^-$  to the Cu UPD deposit, as compared to  $\text{Cl}^-$ , see the discussion in Section 3.4.2. The difference between the CV's in  $\text{Cl}^-$ -containing and  $\text{Cl}^-$ -free electrolyte, see Figs. 3.7 and 3.11a, can be explained using the same argument. The Cu UPD deposition peak in the  $\text{Cl}^-$ -free solution can not be clearly separated into two peaks, as opposed to the electrolyte with  $\text{Cl}^-$ , since the processes of the growth of the UPD patches and the formation of the islands happen almost simultaneously. We cannot, however, unambiguously explain the Cu UPD stripping peak in the  $\text{Cl}^-$ -free electrolyte. Based on the arguments discussed in Section 3.4.2, we think that the observed peak shape is due to a strong incorporation of the SPS into the UPD layer.

### 3.5.2 Further support for the proposed model: lifting of the herringbone reconstruction by Cu UPD

Our model, proposed in the previous subsection, assumes firstly that small gold islands are formed, when the SPS molecules release their gold atoms, and secondly that these small gold islands are stabilized due to the immediate covering by the Cu UPD layer. In addition, when stripping the Cu UPD layer, small gold islands should quickly disappear due to surface diffusion. Larger islands may remain present for some time after the Cu UPD layer stripping.

We test the above points by using the lifting of the herringbone reconstruction of Au(111). This reconstruction contains an excess of Au-atoms of 1 extra atom per 22.5 surface atoms. The reconstruction is lifted in  $\text{SO}_4^-$ - (or  $\text{Cl}^-$ ) containing electrolytes at potentials above approx. 300 mV (150 mV for  $\text{Cl}^-$ ) due to anion adsorption [123]. If  $\text{Cu}^{2+}$  ions are present in the electrolyte, the copper cations are adsorbed at the surface at potentials more negative than the values mentioned above, leading to the Cu UPD layer formation and also preventing the Au(111) surface reconstruction. Thus, the herringbone reconstruction of the Au(111) surface in a  $\text{Cu}^{2+}$ - and  $\text{SO}_4^-$ - (or  $\text{Cl}^-$ -) containing electrolyte generally cannot exist. Note, that lifting of a surface reconstruction by metal UPD has been observed experimentally and is reported in the literature [124–127]. Most of these studies have been conducted on systems, where there is a potential range in the metal-ion-containing electrolyte, at which the surface reconstruction exists.

Similar to the scenario of Fig. 3.13 of our model, we now expect the following. If a freshly prepared, reconstructed Au(111) surface would be immersed into a copper-free, but  $\text{SO}_4^-$ -containing electrolyte under potential control, while keeping the sample potential below 300 mV, the herringbone reconstruction should persist [123]. If afterwards  $\text{Cu}^{2+}$  ions would be injected into the solution, it should force a rapid lifting of the reconstruction. The excess gold atoms should be ejected and should lead to the formation of (metastable) small gold islands. Since at these potentials the Au(111) surface is

covered by the Cu UPD layer, also these islands rapidly should become covered by the Cu UPD layer. This, in turn, should reduce the mobility of the gold, thereby effectively stabilizing the islands.

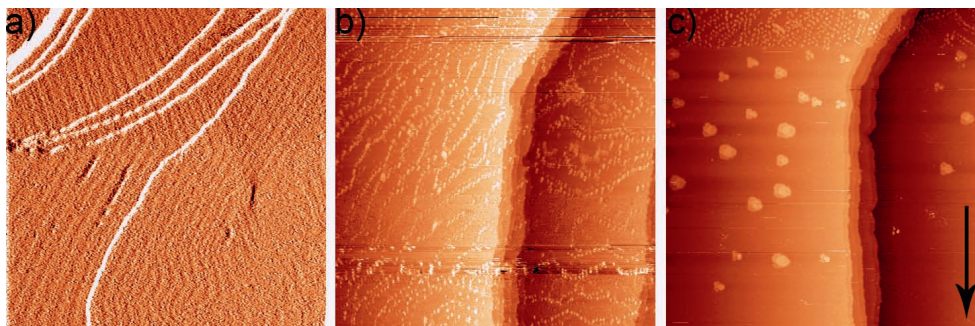


**Figure 3.14:** STM images of the lifting of the herringbone reconstruction by Cu UPD layer formation. (a) Differentiated image of the reconstructed Au(111) surface in 0.1 M  $\text{H}_2\text{SO}_4$  at 200 mV. (b) Au surface after introduction of  $\text{Cu}^{2+}$  ions into the solution at the same potential. Small, monatomically high Au islands are covering the surface. (c) Stripping of the Cu UPD layer by sweeping the potential from 200 mV to 400 mV. The small islands disappear quickly at the top of the image and large islands appear. Note that the clusters on the terraces are imaged with a multiple-tip in (b) and with a triple-tip in (c); the three steps in the images are real. The size of all images is  $250 \times 250 \text{ nm}^2$ . The tunneling parameters are: tip potential between 0 mV and 100 mV, tunneling current between 500 pA and 1 nA.

We have conducted this experiment using our flow-cell, which allows an *in-situ* exchange of electrolytes during STM imaging while maintaining potential control. The STM images at different stages of the experiment can be seen in Fig. 3.14. Figure 3.14a shows the reconstructed Au(111) surface in a Cu-free solution. Afterwards, the Cu-containing electrolyte was pumped into the cell. A network of small islands with the height of a monatomic Au(111) step emerges at the Cu UPD covered Au(111) surface, see Fig. 3.14b. The geometry of the network of islands is reminiscent of that of the herringbone reconstruction. Note that there is a multiple-tip in 3.14b and a triple-tip in 3.14c. Both tip problems affect only the imaging of the smaller clusters on the terraces; the three steps in the images are real. We found it rather difficult to get a stable and sharp tip during the Cu UPD layer formation on the reconstructed Au(111) surface. In Fig. 3.14c the sample potential is swept to a value above the dissolution potential of the Cu UPD layer. The small islands disappear rapidly as soon as the stripping potential is reached, see top of Fig. 3.14c, and some larger gold islands appear. The surface morphologies, observed in Figs. 3.14a, 3.14b, and 3.14c, precisely meet the expectations described above and verify the model proposed in the previous section: small gold islands get indeed stabilized by the Cu UPD layer.

### 3.5.3 Confronting our model with the literature

Analyzing the literature on UPD layer growth on the Au(111) surface that is modified by thiol SAMs, we can further generalize our model. In many studies the UPD growth of Cu [75–77, 91], but also of Ag [87], was found to proceed in distinct steps, starting with a lower-apparent-height deposit (patches) that is followed by the appearance of higher islands on the surface. The nature of these islands has been attributed to bilayers of the UPD deposit forming under the SAM [91], or to the formation of islands of thiol molecules with a more dense structure than the SAM [75, 77], but also to monatomically high gold islands [88] (based on the island height analysis). However, judging from the STM images in [75–77, 87, 91], we argue that the process observed in these studies is the same, or at least very similar, to the one proposed here.

Some authors have observed island formation on thiol SAM-covered surfaces in metal-ion-free solutions, and have claimed that the islands are due to the thiol molecule reorientation at the surface [75]. However, in our studies we have never observed island formation in SPS-containing electrolytes in the absence of  $\text{Cu}^{2+}$ .

## 3.6 Additional observations

In this section we present additional experimental observations to firstly shed light on the interplay between anions coadsorbed during Cu UPD layer formation and adsorbing SPS, and secondly to provide additional support for the general nature of our model.

### 3.6.1 Adsorption of SPS onto pre-grown Cu UPD layers: the effect of anions

In the following we present results on SPS adsorption onto an already formed Cu UPD layer on Au(111) that was grown in the absence of SPS and either in the presence or in the absence of  $\text{Cl}^-$  ions in solution. The motivation for these experiments is threefold. Firstly, we would like to test our explanation for the observed differences between the Cu UPD in SPS-containing solution with and without  $\text{Cl}^-$ , see Section 3.4.2. Secondly, we would like to check whether SPS is coadsorbed during the Cu UPD. Finally, we would like to see whether the structure of the UPD layer with the SPS is different as compared to the UPD layer formed without the SPS.

The experiments were performed as follows. First, the sample was mounted in the STM and brought in contact with an SPS-free solution containing 0.1 M  $\text{H}_2\text{SO}_4$  and 10 mM  $\text{CuSO}_4$  in the  $\text{Cl}^-$ -free case, and additionally 1 mM HCl for the  $\text{Cl}^-$ -containing solution. Then, the Cu UPD layer was grown by setting the sample potential to 170 mV.

While keeping the potential at that value and continuously imaging the surface with the STM, 10  $\mu\text{M}$  SPS was added to the solution.

Figure 3.15a shows an STM image of the Au(111) with a Cu UPD layer in the  $\text{Cl}^-$ -containing solution prior to the injection of SPS. Note that the UPD layer has a low density of defects in the presence of  $\text{Cl}^-$ ; the main sources for defects, such as domain boundaries, are the monatomic steps of the Au(111) surface. Also, the tunneling current exhibits little noise resulting in a smooth appearance of the surface in Fig. 3.15a. Approximately 30 s after the injection of the SPS into the solution<sup>1</sup>, the noise in the tunneling junction increases and the STM image becomes stripy, see Fig. 3.15b. We attribute this observation to the initial adsorption of highly mobile SPS molecules on the UPD layer, but we cannot rule out that the bad image quality is caused by SPS that is bound to the tip and therefore part of the tunneling junction. We define the time at which the image in Fig. 3.15b was taken as  $t = 0$  s, i.e. the time of the onset of the SPS adsorption<sup>2</sup>. Figures 3.15 c and d show snapshots of the surface at  $t = 426$  s and at  $t = 1705$  s respectively. From the images one sees that the Cu UPD layer transforms: the transformation begins at both the upper and the lower parts of the steps as well as the domain boundaries in the UPD layer. From the two different transformation fronts, we can conclude that the transformation proceeds in two steps. First, small spots with diameters between 0.5 nm and 1.5 nm appear on the surface. The average height of these small spots, as measured with the STM, is  $0.14 \pm 0.02$  nm. Then, higher features with diameters of up to 10 nm and heights of  $0.38 \pm 0.08$  nm emerge<sup>3</sup>. It is interesting to notice that the height of the larger features on the transformed part of the UPD layer approximately equals the sum of the height of the smaller spots ( $0.14 \pm 0.02$  nm) and the height of a monatomic step of Cu(111) of 0.21 nm. We can conclude that during the adsorption of SPS, major restructuring of the Cu UPD layer occurs including probably also the formation of a second Cu layer on top of the first one. The whole transformation process is rather slow: even after 30 minutes  $\sim 20\%$  of the surface remains non-transformed.

A possible interpretation of the observed Cu UPD layer transformation is as follows. Shortly after the injection of SPS into the solution, SPS starts to adsorb everywhere on the UPD layer. Since the Cu UPD layer in the  $\text{Cl}^-$ -containing solution is terminated by a densely packed defect-poor  $\text{Cl}^-$  overlayer, the SPS molecules cannot easily reach the metal atoms (either of the Cu UPD layer or of the Au surface) and make a chemical sulfur-metal bond. Hence, we assume that SPS is initially physisorbed on the surface,

---

<sup>1</sup> It is important to realize that right after the SPS injection, the SPS concentration at the sample surface increases gradually due to the diffusion in the liquid cell towards the surface; the surface concentration reaches a constant (bulk) value after approx. 3 minutes.

<sup>2</sup> The times stated here refer to the start of the recording of the STM images

<sup>3</sup> Please note that both the small spots and higher features are different in nature and size from the patches and islands, observed in Section 3.4.1

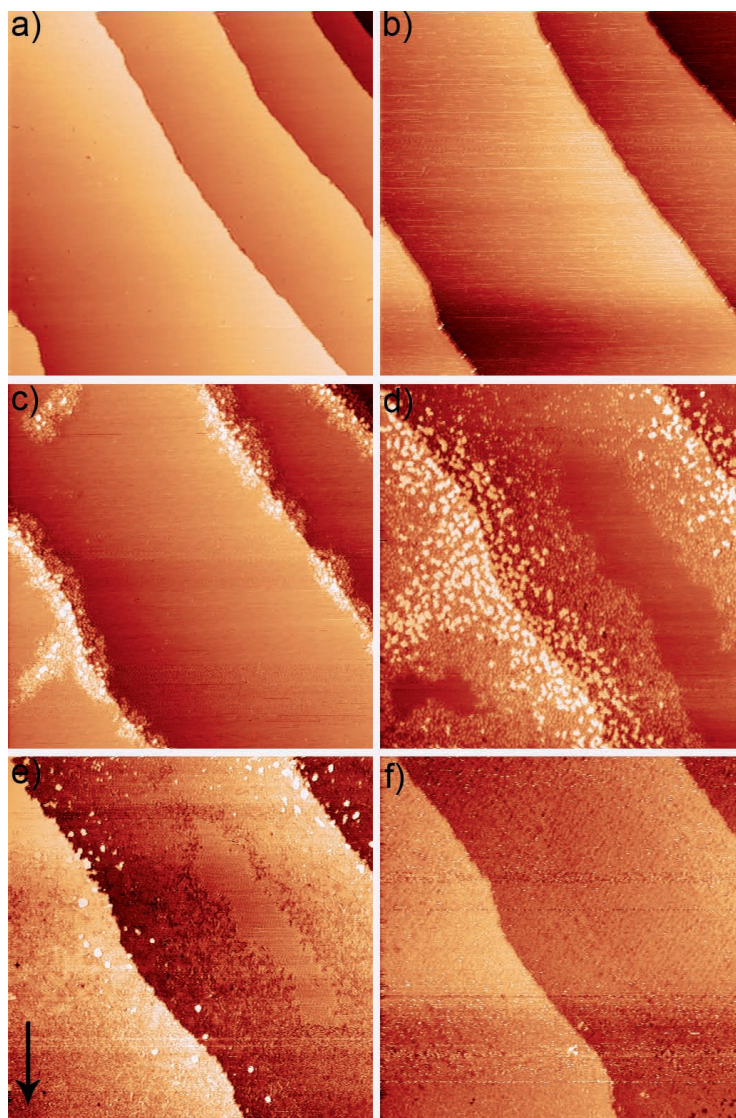


**Figure 3.15:** STM images of SPS adsorption onto a pre-grown Cu UPD layer on Au(111) in a  $\text{Cl}^-$ -containing solution. (a) The complete Cu UPD layer prior to the injection of SPS. (b) The initial adsorption of SPS indicating high mobility. The adsorption results in a slow transformation of the UPD layer with two transformation fronts, as can be seen in (c) after  $t = 426$  s and in (d) after  $t = 1705$  s. The images (a)-(d) are taken at a surface potential of  $170$  mV. In (e) the potential was swept from  $200$  mV to  $280$  mV to strip the UPD layer. The arrow shows the time axis. In the middle of the lower terrace the non-transformed part of the Cu UPD is visible. Note, that although the transformed part of the UPD layer was stripped at around  $230$  mV, the non-transformed part remained stable up to  $265$  mV. (f) The surface at  $300$  mV after complete desorption of the UPD layer. An unstable tip lead to the rough appearance of the terraces. The size of all images is  $200 \times 200 \text{ nm}^2$ .

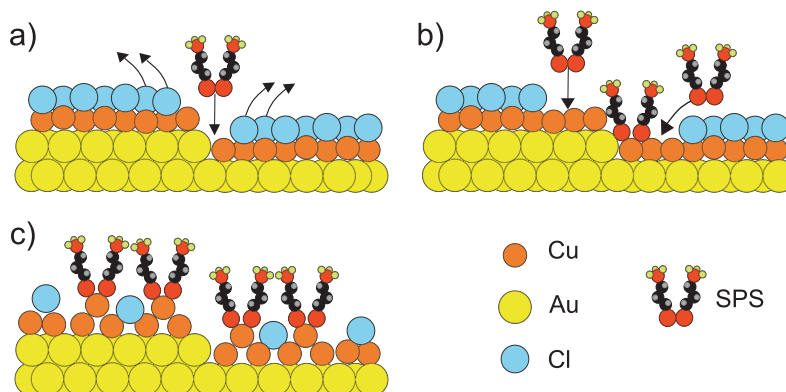


**Figure 3.16:** Model of SPS adsorption onto a pre-grown Cu UPD layer in a  $\text{Cl}^-$ -containing solution. (a) Initial adsorption of SPS molecules in the vicinity of a monatomic step. Cl is desorbed in the vicinity of the adsorbed SPS. (b) Further adsorption of SPS on the uncovered Cu layer. This leads in the appearance of the small spots in the STM images. (c) Additional SPS adsorption results in the redistribution of the Cu atoms within the UPD layer. This results in larger features, as observed with the STM.

leading to the stripy STM image, see Fig. 3.15b. However, at the UPD layer defects, such as domain boundaries and monatomic steps, the metal atoms are not completely covered by the  $\text{Cl}^-$  overlayer, see Fig. 3.16a. Thus, a sulfur-metal bond is readily formed at these locations. This chemical bond changes the electronic properties not only of the metal atoms participating directly in the bond, but also of the atoms in the vicinity of the adsorbed thiol [128]. In turn, this may lead to a weakening of the Cl-Cu bond in the vicinity of an adsorbed SPS molecule, resulting in a partial (or complete) Cl desorption from the UPD layer, as depicted in Fig. 3.16a. This desorption would expose new Cu atoms, which would be otherwise protected by the Cl overlayer, and to which SPS can bind to, see Fig. 3.16b. This mechanism leads to the propagation of the first transformation front of the UPD, i.e. the appearance of the small spots, see Figs. 3.15 c and d. As more SPS molecules are adsorbed, the UPD layer undergoes a second transformation, resulting probably in the rearrangement of the Cu atoms in the layer<sup>1</sup>, see Fig. 3.16c. This rearrangement leads to the second transformation front, resulting in the formation of higher features, as observed in Fig. 3.15d. We think that a part of the original Cl overlayer might remain coadsorbed with the SPS after the transformations.

If the potential is slowly raised towards more positive values, first the transformed part of the UPD layer is stripped at potentials around 230 mV, see Fig. 3.15e. It is not completely clear, whether the transformed UPD layer is stripped completely or whether

<sup>1</sup>Please note that, although we assume that the total number of Cu atoms on the surface remains unchanged, exchange processes between the surface and the solution can take place.

there still remains some deposit. The non-transformed part, see in the middle of the large terrace, of the Cu UPD layer seems to be unchanged until the potential is further raised to 265 mV. Above 265 mV the complete UPD layer is removed independently whether it was transformed or not. Right after stripping at a potential of 300 mV, the Au(111) surface appears rather disordered, see Fig. 3.15f. We think that this is due to adsorption of the SPS onto the Au surface, accompanied by the creation of vacancies, see Section 3.5.1. An indication for this is given by the fact that, after some time, the Au surface becomes similar to the one shown in Fig. 3.9b, exhibiting larger vacancy islands and domain patches of an ordered SAM.

If there is no  $\text{Cl}^-$  present in the solution, the adsorption of the SPS onto a pre-grown Cu UPD layer proceeds differently. Figure 3.17a shows an image of the surface at the onset of the SPS adsorption. The adsorption of the SPS and consequently the transformation of the UPD layer proceeds much faster without  $\text{Cl}^-$ : after around 220 s the transformation is complete, whereas in the  $\text{Cl}^-$ -containing solution the transformation is not finished even after 1800 s. At the bottom of Fig. 3.17a the UPD layer is still intact, but at the top, after approximately 80 s, patches of transformed regions start to appear. Note, that the transformation in the  $\text{Cl}^-$ -free solution is different from the  $\text{Cl}^-$ -containing case, as it proceeds only with one transformation front, see Fig. 3.17b. The nucleation of the transformed regions occurs at the UPD layer defects. Since the Cu UPD layer in the solution without  $\text{Cl}^-$  contains more defects than the UPD with  $\text{Cl}^-$ , see Fig. 3.3a, the nucleation density is higher and nucleation occurs not only at the monatomic steps but also at defects on the flat terraces. The height of the transformed layer is  $0.13 \pm 0.02$  nm. Please note that, within the error margin, the heights of these transformed regions and the small spots in Fig. 3.15 are the same. In addition, higher features start to appear on the transformed UPD layer that might be compared with the features of the second stage of the transformation in the  $\text{Cl}^-$ -containing case, see Fig. 3.17d. Please note one significant difference: the larger features are formed during a second transformation behind a moving front in the  $\text{Cl}^-$ -containing case, whereas here the features occur "everywhere" on the transformed UPD layer. We measure the height of the features to be  $0.40 \pm 0.06$  nm. Their lateral size is between 1 nm and 2 nm, which is smaller than the size of the similar features in the  $\text{Cl}^-$ -containing electrolyte.

As mentioned above, the transformation of the UPD layer in the  $\text{Cl}^-$ -free solution starts at surface defects, such as domain boundaries and monatomic steps, and proceeds in a generally similar way, as in the  $\text{Cl}^-$ -containing electrolyte. Thus, we assume that the atomic processes responsible for the transformation in the  $\text{Cl}^-$ -free solution may be described by the model in Figs. 3.16 a and b. However, the second transformation front is not observed in the  $\text{Cl}^-$ -free solution. We propose that the reason for that are the different initial values of the surface coverage of Cu in the UPD layer in  $\text{Cl}^-$ -containing and  $\text{Cl}^-$ -free electrolytes: it amounts to 0.75 of a monolayer with  $\text{Cl}^-$  and to 0.66 of

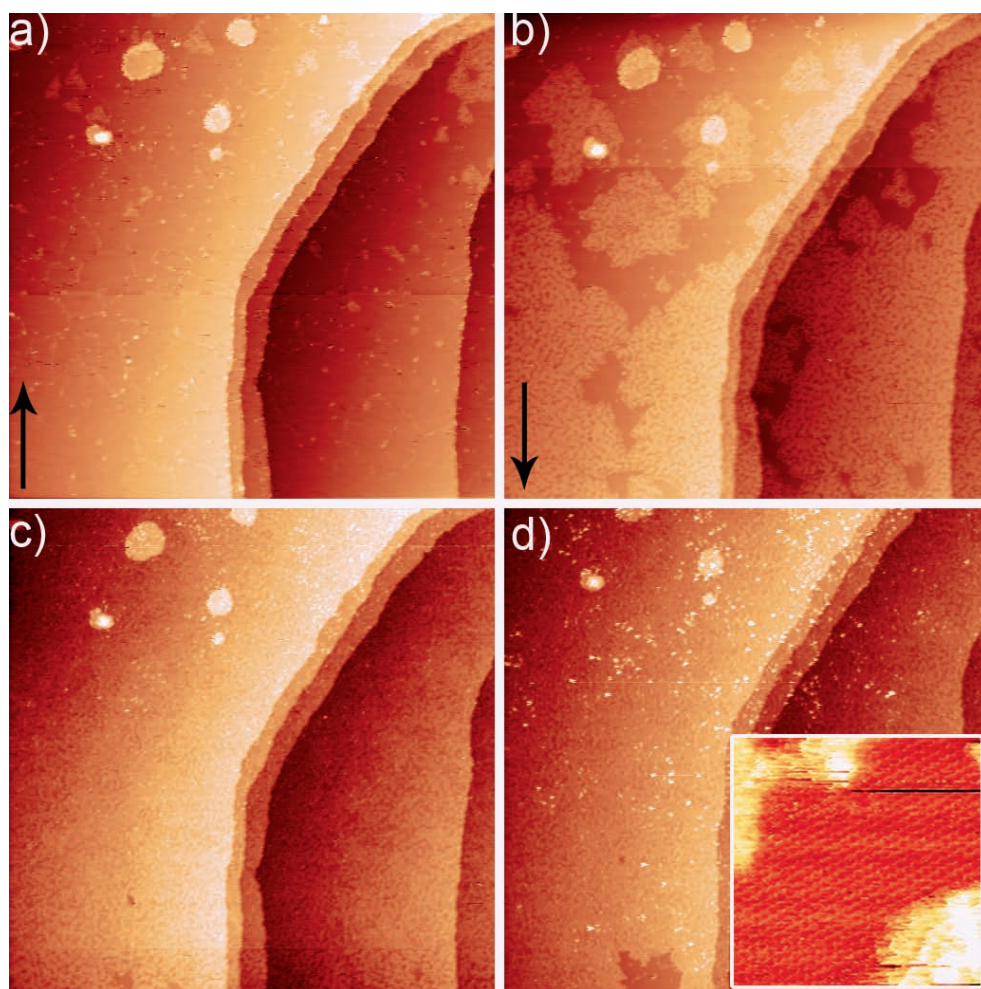


**Figure 3.17:** STM images of SPS adsorption onto a pre-grown Cu UPD layer in a  $\text{Cl}^-$ -free solution. In (a), (b) and (c) are three consecutive images, displaying the SPS adsorption process. SPS was injected into solution before image (a) was taken. Image (a) was acquired with a rate of 120 s/image and images (b) and (c) were acquired with a rate of 87 s/image. (d) shows the surface  $t = 860$  s after the onset of adsorption. Higher features are visible. The inset in (d) shows a zoom-in onto a non-transformed part of the surface. Note, that the surface drifted about 30 nm in the vertical direction between images in (c) and (d). All images were acquired at a surface potential of 170 mV. Images (a)-(d) have a size of  $250 \times 250 \text{ nm}^2$ , and the inset in (d) has a size of  $12 \times 12 \text{ nm}^2$ . The tunneling parameters are: 52 mV tip potential, and 300 pA tunneling current.

a monolayer without  $\text{Cl}^-$  but with sulfate<sup>1</sup> [23, 103, 112]. If we assume that the final surface coverage of Cu after the SPS adsorption on the UPD layer is the same in both cases, more Cu atoms are expected to be expelled from the layer in the solution with  $\text{Cl}^-$ . This could explain the formation of the features during the second transformation step, see Figs. 3.15 c and d.

Based on the above described observations, we can conclude that SPS *does* adsorb on the Cu UPD layer in both cases, i.e. with and without  $\text{Cl}^-$  in the solution. This also strongly suggests that during the formation of the Cu UPD layer in the presence of the SPS in the solution, additional SPS is coadsorbed leading to a possible incorporation into the UPD layer. Obviously, the structure of the UPD layer with SPS must be different than without SPS, despite a good match between the charge densities associated with the UPD layer formation in the SPS-free and SPS-containing solutions, see Section 3.4.1.

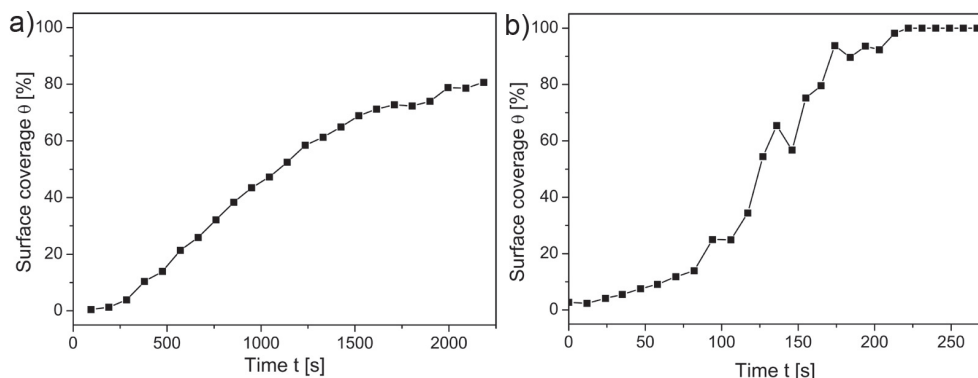


**Figure 3.18:** Time evolution of the relative surface coverage of the transformed part of the Cu UPD layer at surface potential of 170 mV in: (a)  $\text{Cl}^-$ -containing electrolyte (first transformation front); (b)  $\text{Cl}^-$ -free electrolyte.

Let us in the following consider the time needed for the transformation of the Cu UPD layer after SPS injection of both the  $\text{Cl}^-$ -free and  $\text{Cl}^-$ -containing solutions, see Fig. 3.18. The transformation (and related adsorption) proceeds one order of magnitude faster in the solution without  $\text{Cl}^-$ . The adsorption of the SPS must be accompanied by the displacement and/or desorption of the anions that are bond with the UPD layer. The kinetics of the SPS adsorption is, therefore, influenced by the binding energy of the anions to the Cu of the UPD layer: the stronger the anion binds to the Cu of the UPD layer and the smaller the difference in binding energy is between the SPS and the anion to the Cu, the slower will be the SPS adsorption and the UPD transformation. This trend is reflected in 3.18, where the transformation occurs much slower for the  $\text{Cl}^-$ -containing

<sup>1</sup>A monolayer corresponds to the surface concentration of gold atoms of an ideal (111) surface.

case. Indeed, we expect the UPD with  $\text{Cl}^-$  more stable, as Cl binds stronger to copper than sulfate, see Section 3.4.2. In addition, the Cl bond to Cu is only slightly weaker than the thiol-copper bond.

Finally, let us discuss the model from Section 3.5.1 in the light of our results on SPS adsorption on a pre-formed Cu UPD layer. In the model we have assumed that, during the initial stages of Cu UPD, the growing Cu UPD patches are covered with  $\text{Cl}^-$  (or  $\text{SO}_4^{2-}$ ), whereas the thiol molecules stay only adsorbed on the Au(111) surface via gold adatoms, see Fig. 3.13c. However, the new insights of the present subsection indicate that our model is inaccurate with respect to the formation of the Cu UPD patches, as we have clearly shown that SPS adsorbs on a pre-formed SPS-free Cu UPD layer.

One has to remember that in our electrolyte compositions, which we used throughout this chapter, we have a  $10^4$  times higher  $\text{SO}_4^{2-}$  concentration and, in a  $\text{Cl}^-$ -containing solution, a 100 times higher  $\text{Cl}^-$  concentration, than the concentration of SPS. On the other hand, the formation of the Cu UPD layer is a fast process, as we have shown in Fig. 3.6c. Thus, the species that are abundant are expected to preferentially coadsorb with  $\text{Cu}^{2+}$  during the initial formation of the UPD patches. This justifies our assumption that the Cu UPD patches are initially covered with  $\text{Cl}^-$  (or  $\text{SO}_4^{2-}$ ). Furthermore, it is rather naive to assume that the SPS molecules stay bound to Au adatoms until they are squeezed enough to be able to leave the adatoms. More realistically, for every coverage of the surface by the Cu UPD patches there is a certain rate of SPS detachment from the Au adatoms, which increases with the decreasing potential (increasing coverage by the UPD patches) and reaches its maximum at the potential of peak "II" in Fig. 3.7. If this is the case, only one peak should be visible in the CV for Cu UPD layer formation, if the potential sweep rate is slow enough to allow the system to approach equilibrium at each potential value. Indeed, this is exactly what we observe, see Fig. 3.19.

Using the above considerations, as well as the results of this subsection, we come up with two possible scenarios of the Cu UPD layer formation. We will start with the description of the first scenario. At the initial stages of the UPD layer formation in the presence of SPS, the UPD patches consist of a Cu layer with coadsorbed  $\text{Cl}^-$  (or  $\text{SO}_4^{2-}$ ) overlayer, see Fig. 3.20a. As these patches grow out, more and more SPS molecules leave their Au adatoms and diffuse onto the UPD layer, probably displacing the Cl atoms. This should lead to the transformation of the UPD layer, similar to what is shown in Figs. 3.15c-d and 3.16. In our experiments on SPS adsorption on a preformed Cu UPD layer in a  $\text{Cl}^-$ -containing solution, we have attributed the second transformation front to such a transformation. However, we do not see any transformation of the Cu UPD patches that grow on a Au(111) surface in the presence of SPS, see Figs. 3.9a and c. We propose that we do not see such transformation, since the change of the structure of the Cu UPD patches due to SPS is accompanied by a lateral spread of the patches, which is depicted in Fig. 3.20b. Such a lateral spread is impossible in the case of SPS

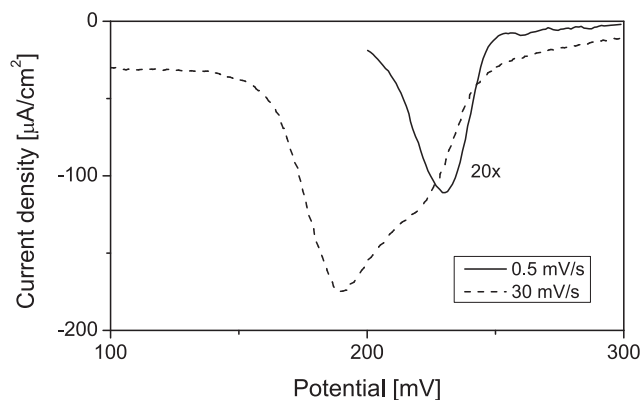


**Figure 3.19:** Linear sweep voltammograms of Au(111) in a solution containing 0.1 M  $\text{H}_2\text{SO}_4$ , 10 mM  $\text{CuSO}_4$ , 1 mM HCl, and 10  $\mu\text{M}$  SPS acquired at 30 mV/s (dashed line) and 0.5 mV/s (solid line) sweep rates from higher to lower potential. At the fast sweep rate, the double-peak of Cu UPD is observed, whereas at the slow sweep rate, a single peak is found.

adsorption on a preformed Cu UPD layer, thus the excess Cu atoms are redistributed within the layer, leading to the observed second transformation front, see Figs. 3.15c-d.

Although the concentration of SPS in our experiments is much smaller than the concentration of the anions, we still cannot rule out the coadsorption of SPS from the solution during the initial formation of the Cu UPD patches. Hence, we propose an alternative scenario, which could both fit our model from Section 3.5 and the results of this subsection, and also takes into account the coadsorption of SPS with Cu during the UPD. Let us assume that initially the Cu UPD patches are covered with the coadsorbed SPS molecules as well as with the coadsorbed anions, see Fig. 3.20c. The patches have the structure of the final, completed Cu UPD layer with SPS. As the potential is lowered, the patches grow out, forcing the SPS molecules adsorbed on Au to leave their Au adatoms. The molecules then either desorb into the solution, as they cannot diffuse onto the Cu UPD layer, which is already occupied by SPS molecules, or they diffuse onto the edges of the growing UPD patches, which are not yet covered with the SPS adsorbed from the solution, see Fig. 3.20d.

Thus, we have shown that the results of our experiments presented in this section can be used to complement our model of Cu UPD layer formation in the presence of SPS. Although, the model is probably correct in general, the particular details of the UPD layer formation process still remain uncertain. One possibility to get more details on the process is to study the Cu UPD layer formation in solutions with different SPS concentrations, as an extremely low concentration would result in the first scenario of Fig. 3.20, whereas a high SPS concentration would probably favor the second scenario.

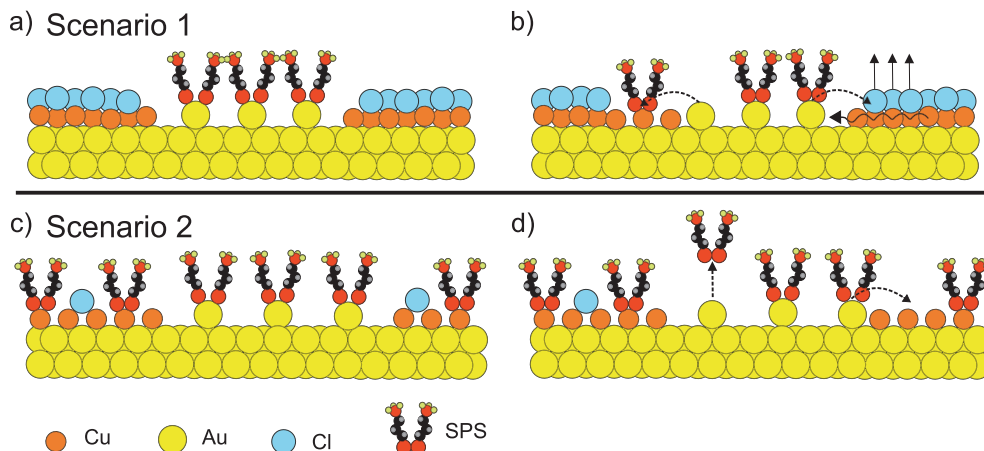


**Figure 3.20:** Two possible scenarios for the growth of the Cu UPD patches on Au(111) in the presence of SPS. In the first scenario, the UPD patches are initially covered by the coadsorbed Cl<sup>-</sup> (or SO<sub>4</sub><sup>2-</sup>) (a). As the patches grow out, the SPS molecules detach from their Au adatoms and diffuse onto the UPD patches, leading to the Cl<sup>-</sup> desorption and the transformation of the UPD structure (b). The transformation leads to the lateral spread of the UPD patches. In the second scenario, the UPD patches are initially covered by the coadsorbed SPS. As they grow, the SPS molecules, which are bound via Au adatoms to the Au surface, are either desorbed to the solution, or diffuse onto the edges of the growing Cu patches, which are not yet covered with the SPS (d).

### 3.6.2 Cu UPD on a hexanethiol-modified Au(111) surface

In Section 3.5 we proposed a model of Cu UPD on Au(111) in the presence of SPS and claimed, in addition, that our model is of more general nature and holds for metal UPD in the presence of different thiol-like molecules. In this section we present further experimental support to our claim by measurements of Cu UPD on a Au(111) surface that has been modified by a SAM of hexanethiol (C6).

Already here we would like to mention that the results in this subsection should be taken with some caution, as we found a strong influence of the tip on the processes observed with the STM<sup>1</sup>, see also Appendix B. Figure 3.21 shows the CVs of the Au(111) surface in the presence of C6. At a tip potential of 50 mV we observe the formation of the Cu UPD layer under the tip at the surface potential of 450 mV, which is about 200 mV more positive than the closest deposition peak in the CV's of the system, see Fig. 3.21. Thus, the tip probably changes the surface potential locally in the area being imaged. We also found that the magnitude of this local surface potential shift is dependent on the tip potential. However, we did not study this dependence systematically. Further, our

<sup>1</sup>No tip influence was observed in the case of SPS.

STM measurements at different tip potentials suggest that the general process of the Cu UPD layer formation, i.e. growth of patches and subsequent appearance of islands, remains unaffected by the vicinity of the tip. All measurements presented further in this subsection were conducted with a tip potential of +50 mV.

Concerning the influence of C6 on the Cu UPD formation, we performed two sets of experiments: in the one case the C6 were pre-adsorbed on Au(111) followed by an experiment using a C6-free solution, whereas in the other case we used a solution containing the C6 directly. In the first case, we have prepared a SAM of C6 by immersing the Au(111) single crystal into a C6-containing ethanol solution for  $\sim 24$  hours with subsequent rinsing in ethanol and in ultra-pure water, following a procedure described in Ref. [75]. After that the sample was mounted into the electrochemical cell and exposed to a C6-free electrolyte. The C6-free electrolyte composition was 0.1 M  $H_2SO_4$ , 10 mM  $CuSO_4$ , and 1 mM HCl in ultra-pure water. In the other case, we have exposed the crystal directly to a C6-containing aqueous electrolyte. Despite the poor solubility of C6 in aqueous solutions (solubility in water 0.047g/l), we could achieve a concentration of  $\sim 2 \mu M$ . Based on our studies of the SAM's of SPS, as well as from experiments found in literature [129], this concentration should be high enough for producing a C6 SAM on Au(111). Please note that, referring to literature, the latter method is barely used for the formation of an alkanethiol SAM. With the STM we did not observe a difference between the SAM's prepared by the two different methods.

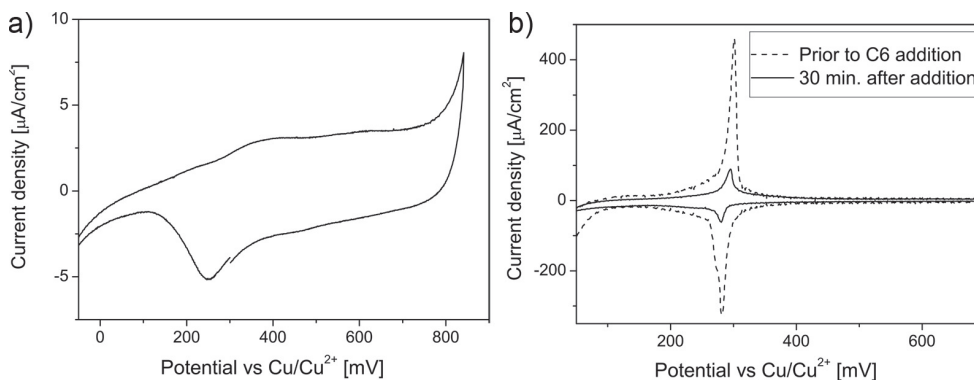


**Figure 3.21:** CV's of Au(111) crystals, covered with SAM's of C6, which were prepared in two different ways. (a) The C6 SAM was prepared by immersion into a  $2 \mu M$  C6 solution in ethanol for 48 hours. The CV in (a) is measured in a solution containing 0.1M  $H_2SO_4$ , 10mM  $CuSO_4$ , and 1 mM HCl. (b) The SAM was prepared by the addition of  $20 \mu M$  C6 directly into the same solution as in (a), which was in contact with a C6-free Au(111) crystal. The CV's in (b) were acquired prior to C6 addition to the solution (dashed line) and 30 minutes after adding C6 (solid line). The potential sweep rate is 30 mV/s.

Figure 3.21a shows a CV of Au(111), pre-covered with a SAM of C6, in the C6-free

electrolyte. A decrease of the Cu UPD deposition and dissolution peak currents and of corresponding transferred charges by two orders of magnitude, as compared to the CV of a C6-free surface (Fig. 3.4), indicates good passivation of the gold surface by the C6 molecules. In fact, it has been shown that alkanethiol SAM's act as barriers for metal deposition onto metallic surfaces [76, 87]. A broad deposition peak found between 400 mV and 150 mV is distinguishable in the CV, which can be assigned to the Cu UPD; this peak is not observed in Cu-free electrolyte. We attribute this peak to the Cu UPD layer formation at the defects of the SAM and/or possible contaminants since the charge<sup>1</sup> of  $\sim 9 \mu\text{C}/\text{cm}^2$ , associated with this peak, makes up only  $\sim 3\%$  of the charge of  $360 \mu\text{C}/\text{cm}^2$ , transferred during the UPD layer formation on a clean Au(111) surface. Also note that the capacitive currents in the double-layer region are decreased roughly by a factor of 3 for the C6-covered surface, as compared to the clean Au(111) surface. This decrease can be explained by the decrease of the double-layer capacitance due to the C6-layer adsorption that leads to an increase of the double-layer width.

Figure 3.21b shows a CV of Au(111) in the C6-containing aqueous electrolyte. After approximately 30 minutes of exposure, the Cu UPD current peaks are suppressed. The charge density of the UPD layer formation amounts to  $70 \mu\text{C}/\text{cm}^2$ , which is smaller the charge density associated with the UPD layer formation on a C6-free Au(111) surface. However, the Cu UPD peak position on the potential axis remains almost unchanged, as compared to the clean Au(111) surface. Also, its height as well as the area under the peak are significantly larger compared to the peak found in the CV of the Au(111) in the C6-free electrolyte, but pre-covered with a SAM of C6. A possible reason for this observation might be that a SAM of C6 that is prepared from the aqueous solution contains either significantly more defects (e.g. in the form of domain boundaries) or does not completely cover the entire surface.

It is important to mention here the irreproducibility of the CV's, as has been also reported in the literature [130, 131]. Firstly, there is a strong variation in the shape of the CV's even during the very first potential sweeps for the C6 pre-covered Au(111) case. Secondly, in the cases of the C6 pre-covered Au(111) CV's constantly change upon subsequent sweeping of the potential, even if the potential range is decreased such that no oxidative or reductive desorption of the thiols is expected. Thirdly, we always observed dramatic changes in the CV's when the potential reaches the value of copper bulk deposition.

Figure 3.22a shows a typical STM image of Au(111) in the C6-containing aqueous electrolyte 30 minutes after the addition of C6 to the solution. We would like to mention here that the STM images of Au(111), pre-covered with a SAM of C6, in the C6-free electrolyte looked essentially the same. We observe monatomically deep vacancy islands

---

<sup>1</sup>Please note that this charge value is only approximate, since it is difficult to distinguish the UPD peak from the double-layer (re)charging currents in the CV.

with a Au(111)-step height. These vacancy islands are characteristic for thiol adsorption on metal surfaces, see Section 3.4 and [72–74]. The areal fraction of the vacancy islands ranges from 6% to 12%, which is in good agreement with the literature [68]. The areas between the vacancy islands and the surface at the bottom of the vacancy islands are covered by several differently ordered SAM domains.

Two different SAM structures can be observed in Fig. 3.22b that is acquired at 520 mV. The first structure has a hexagonal arrangement of the molecules with a nearest neighbor distance of  $1.18 \text{ nm} \pm 0.21 \text{ nm}$ . In the second structure, the molecules are aligned in stripes. The distance between the stripes is  $1.72 \text{ nm} \pm 0.32 \text{ nm}$ . The distance between the single molecules within the stripes is  $0.46 \text{ nm} \pm 0.06 \text{ nm}$ . If the potential of the sample is changed to more positive values (up to 800 mV), the whole surface becomes covered by the hexagonal-like SAM structure, whereas the striped structures prevails, if the potential is changed to more negative values. On first sight, one might have the impression that these structures have different C6 densities. However, as the structural change is fully reversible upon several potential cycles in the C6-free electrolyte, there is probably no C6 desorption into the bulk electrolyte.

Upon the decrease of the sample potential to  $\sim 450 \text{ mV}$  small patches start to nucleate and grow on the terraces (see Fig. 3.22c), similar to those described in Section 3.4.1. The patches observed here have a height of  $0.11 \pm 0.02 \text{ nm}$ , which is comparable to the height of  $0.10 \pm 0.03 \text{ nm}$  of the patches, observed with the SPS. Similar to the observations in Section 3.4.1, the patches nucleate on the terraces, and not preferably on the steps or surface defects (in contrast to the thiol-free surfaces). We expect the patches to nucleate at the domain boundaries of the C6 SAM, similar to the observations in Section 3.4.1. If the potential is lowered to  $\sim 430 \text{ mV}$ , the patches grow together and islands with a height of  $0.23 \pm 0.02 \text{ nm}$  appear, see Figs. 3.22 c and d. As in the case of the SPS, this height corresponds well to a monatomic step on Au(111) of  $0.235 \text{ nm}$ . Closer inspection shows that these islands nucleate at the surface positions between the patches, as also happens in the SPS case. The lateral size of these higher islands increases upon further reduction of the potential. The lateral growth stops when the Cu UPD layer formation is finished. Also, the vacancy islands, observed prior to the Cu UPD layer formation (Fig. 3.22a) become smaller and some even disappear completely during the growth of the patches and the nucleation and growth of the higher islands<sup>1</sup>. Figure 3.22d shows an STM image at the surface potential of 350 mV after the completion of the Cu UPD layer formation. As in the case of the SPS, the surface is covered with islands with a monatomic Au(111) step height. Also, several vacancy islands are visible.

To ensure that the observed processes are due to Cu UPD layer formation and not

<sup>1</sup>This is not observed in the case of Cu UPD in the presence of SPS.

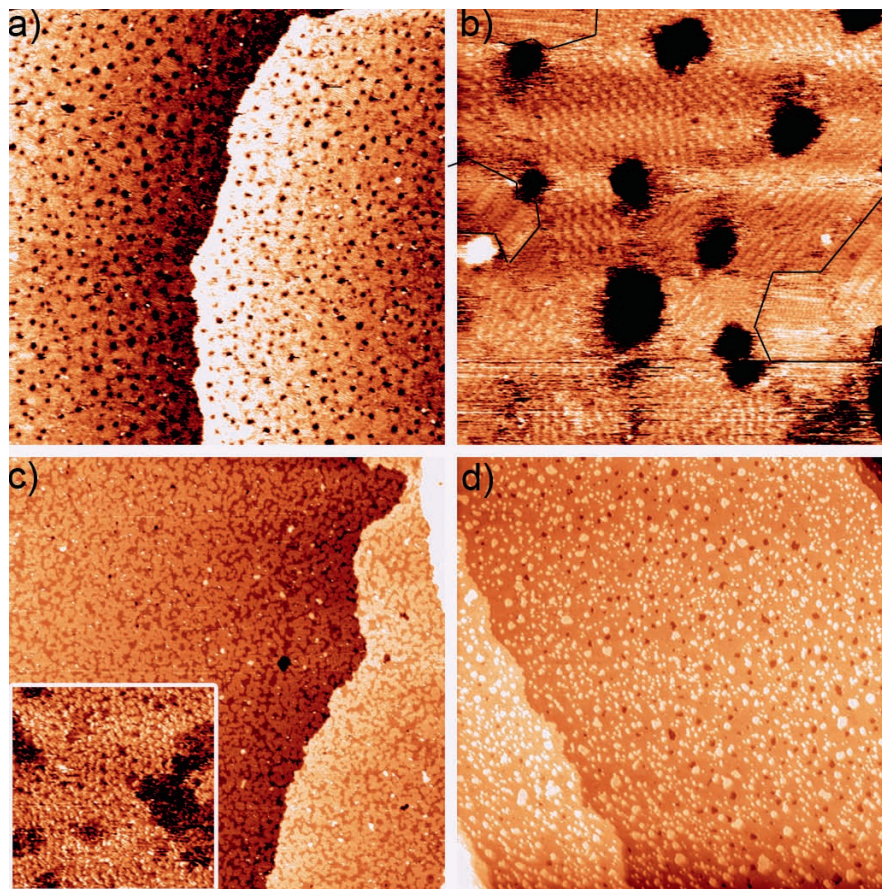


**Figure 3.22:** STM images of Au(111) in  $0.1M H_2SO_4/10mM CuSO_4/1mM HCl$  and  $\sim 20 \mu M$  C6. (a) Large scale STM image of the surface covered with a SAM of C6 at a sample potential of  $590 mV$ . The image size is  $220 \times 220 nm^2$ . (b) Zoom-in at the C6 SAM at a sample potential of  $520 mV$ . Two different SAM structures are visible. Domains with the striped structure are marked by black lines. The image size is  $50 \times 50 nm^2$  (c) Cu UPD patches formed at a sample potential of  $450 mV$ . Inset: zoom-in at the patches, showing a disordered structure. The image size is  $400 \times 400 nm^2$  and that of the inset is  $15 \times 15 nm^2$  (d) Islands with a monatomic Au(111) step height at  $350 mV$ . The image size is  $500 \times 500 nm^2$ . The tunneling parameters are:  $50 mV$  tip potential, and  $300 pA$  tunneling current.

due to e.g. tip influence on the SAM of C6, we have performed also EC-STM measurements on a Au(111) surface, pre-covered with a SAM of C6, in the whole potential range between  $540 mV$  and  $-60 mV$  in a Cu-free electrolyte, i.e. with  $0.1 M H_2SO_4$  and  $1 mM HCl$  only. We never observed any patch or island growth. After adding the  $Cu^{2+}$  ions to

the solution, we could again observe first the formation of the patches at 450 *mV* and further formation of the islands with a monatomic Au(111) step height at slightly lower potentials. Thus the observed patches and islands must be due to the Cu UPD layer formation in the presence of the C6.

Comparing the results of this section with the ones presented in Section 3.4.1, we definitely can conclude that the Cu UPD layer growth processes in the presence of SPS or C6 are essentially the same: first one observes nucleation and growth of patches and upon coalescence of them higher islands with a height of a Au(111) step appear. This confirms the general character of our model and allows its direct application also to the Cu UPD on a C6-modified Au(111) surface.

### 3.7 Conclusions and outlook

We studied the Cu UPD on the Au(111) in a SPS-containing electrolyte. We showed that the deposition proceeds in two distinct steps: firstly, we observe UPD patch formation and growth followed by the appearance of islands with a height of a monatomic Au(111) step during the coalescence of the patches. We argue that these islands appear due to the desorption of thiol molecules that were initially bound to gold adatoms. When disengaged from the thiol molecules during the formation of the Cu UPD layer, these gold adatoms aggregate to small monatomically high gold islands that are immediately covered and stabilized by a Cu UPD deposit on top. This leads to the appearance of islands on a fully closed Cu UPD with a height corresponding to a Au(111) step. Based on our observations, we proposed a model.

In addition, we provided arguments that all point towards a more general nature of our model. We showed that the model still holds for the formation of the Cu UPD layer on Au(111) with different anions in the solution: the UPD layer formation is essentially the same in a  $\text{Cl}^-$ -containing and  $\text{Cl}^-$ -free electrolyte. The slight differences observed in the experiments could be explained by the differences in the binding energies of  $\text{SO}_4^{2-}$ ,  $\text{Cl}^-$ , and SPS to the Cu UPD layer. This was confirmed by comparing theoretically determined values of binding energies of the different species found in literature as well as by conducting SPS adsorption experiments onto the pre-grown Cu UPD layers in different electrolytes. Furthermore, we showed that the model also applies to the formation of the Cu UPD layer on Au(111) in presence of another thiol (other than SPS), such as the hexanethiol.

If we paraphrase our model, we can say that the Cu UPD lifts the surface reconstruction, induced by the thiol molecules. We also showed that, if we grow a Cu UPD layer on a clean Au(111) surface that is naturally reconstructed, i.e. it exhibits the herringbone reconstruction, small islands appear on the surface, similar to those observed in the SPS-containing electrolyte. As these islands clearly get stabilized by a covering

layer of the Cu UPD, this result further supports our model.

We have shown in the SPS injection experiments onto a pre-formed Cu UPD layer that the structure of this layer changes due to the adsorption of the SPS. The results of these experiments show that the details of our model have to be further refined. We propose two specific scenarios of the Cu UPD layer formation that are consistent with the results of the SPS injection experiments and also provide additional details for our model. To supply further proof of the general nature of our model, other systems and thiols should be studied. In addition, it is not clear how exactly the thiol molecules behave during the formation of the UPD layer. From the injection experiments we have evidence that the thiols get incorporated into the UPD layer, but if present before some might also desorb. Further experiments are required to shed light on these questions. In the next chapter of this thesis we address one of these points: we investigate the orientation of the SPS molecules during the Cu UPD.

Finally, even though this chapter provides an extensive view on the role of SPS in the Cu UPD process on Au(111), the treatment is largely descriptive and we necessarily refrain from making quantitative statements at this stage. For example, we addressed the question of a dithiol vs. a monothiol linkage of the molecule to the surface, it was not possible to distinguish which of the two mechanisms was dominant, due to the large error margin in our data. It would be possible to address this question with better statistics.

